CHALMERS
UNIVERSITY OF TECHNOLOGY

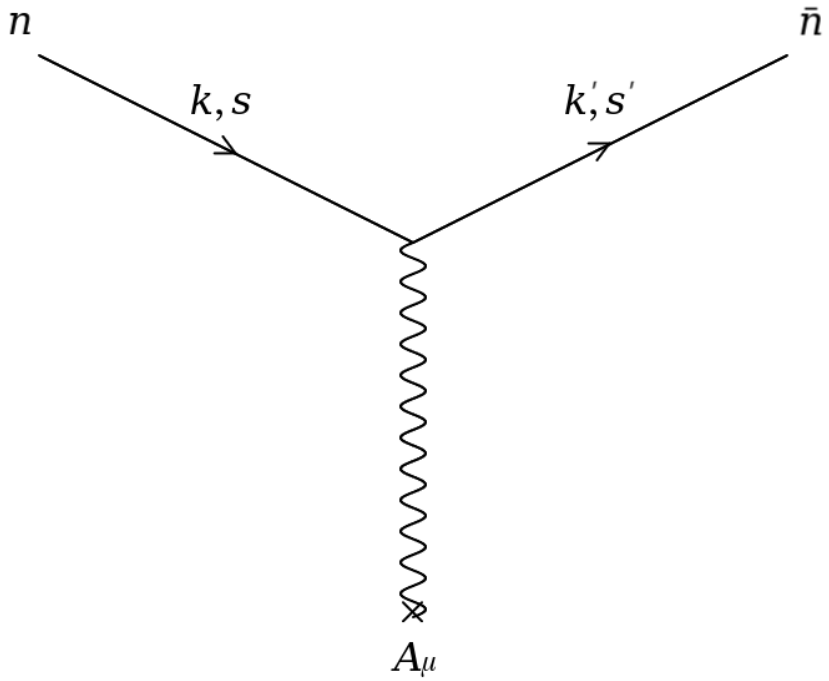

Searching for Vector Wave Dark Matter with Levitated Magnetomechanics

Analysis of a Hypothetical Direct Detection Experiment Using Levitating Superconductive Test Objects

Master's thesis in Physics

MÅNS ANDURI

DEPARTMENT OF PHYSICS

CHALMERS UNIVERSITY OF TECHNOLOGY
Gothenburg, Sweden 2023
www.chalmers.se

Master's thesis 2023

Searching for Vector Wave Dark Matter with Levitated Magnetomechanics

Analysis of a Hypothetical Direct Detection Experiment Using Levitating Superconductive Test Objects

MÅNS ANDURI

CHALMERS
UNIVERSITY OF TECHNOLOGY

Department of Physics
Division of Subatomic, High Energy and Plasma Physics
Theoretical Subatomic Physics Group
Chalmers University of Technology
Gothenburg, Sweden 2023

Searching for Vector Wave Dark Matter with Levitated Magnetomechanics
Analysis of a Hypothetical Direct Detection Experiment Using Levitating Superconductive Test Objects
MÅNS ANDURI

Supervisor: Riccardo Catena, Physics
Examiner: Riccardo Catena, Physics

Master's Thesis 2023
Department of Physics
Division of Subatomic, High Energy and Plasma Physics
Theoretical Subatomic Physics Group
Chalmers University of Technology
SE-412 96 Gothenburg
Telephone +46 31 772 1000

Cover: Feynman diagram showing neutrons scattering against an external vector wave dark matter field.

Typeset in LaTeX
Printed by Chalmers Reproservice
Gothenburg, Sweden 2023

Searching for Vector Wave Dark Matter with Levitated Magnetomechanics
Analysis of a Hypothetical Direct Detection Experiment Using Levitating Superconductive Test Objects
MÅNS ANDURI
Department of Physics
Chalmers University of Technology

Abstract

This master's thesis investigates the sensitivity of a hypothetical direct detection experiment using levitated magnetomechanics for a vector bosonic wave dark matter candidate. The sensitivity studies done is for masses between $1.24 \cdot 10^{-13}$ eV and $4.14 \cdot 10^{-12}$ eV and with four different possible background terms, where the background is assumed to be thermally based. The vector boson is described with the Lagrangian, $\mathcal{L} = -\frac{1}{4}F_{\mu\nu}F^{\mu\nu} - \frac{1}{2}m_{\mathrm{DM}}^2 A_\mu A^\mu + gA_\mu \bar{n}\gamma^\mu n$, and couples to the baryon number minus the lepton number, thus yielding an EP-violating force on a charge-neutral test object. Since it is ultralight it can be seen as a classical wave. To measure the sensitivity, the exclusion and discovery limits for the coupling constant, g, are asymptotically derived with the Asimov data set for 95% confidence interval and the 5σ level respectively. The limits are plotted against the mass scanned over and compared with the discovery limit for an optomechanical experiment for the same dark matter candidate. It is shown that the sensitivity for the most optimistic background is comparable with said experiment.

Keywords: Asimov data set, direct detection, discovery limit, EP-violation, exclusion limit, experimental sensitivity, levitated magnetomechanics, ultralight dark matter, vector boson, wave dark matter.

Acknowledgements

In this last year of working on this master's thesis I have leaned on the support from my friends and family, and for that I thank them. But of course my biggest thanks goes to Riccardo Catena, my supervisor during this project, who has been able to help with all sorts of problems that have come up during the research for and writing of this thesis. I also want to thank Witlef Wieczorek who has explained the potential experiment with levitated test objects and answered my last-minute questions regarding it. And finally I want to thank Amanda Carlsson Salomon for the discussions regarding this thesis and the immense help that this has been.

Måns Anduri, Gothenburg, November 2023

Contents

List of Acronyms

Below is the list of acronyms that have been used throughout this thesis listed in alphabetical order:

CDF	Cumulative distribution function
CTH	Chalmers tekniska högskola (Chalmers University of Technology)
DM	Dark matter
EP	Equivalence principle
MACHO	Massive astrophysical compact halo object
PDF	Probability density function
PSD	Power spectral density
WIMP	Weakly interacting massive particles
SHM	Standard Halo Model
QFT	Quantum field theory

1

Introduction

Dark matter is a great unknown in physics. It makes up the majority of matter in the known universe, and yet its constituent parts are still undetermined. Discovery of dark matter could have huge consequences in astronomy and particle physics. A better understanding of what the universe is made of would also have an indirect effect on society, in popular culture, and technology, and it could lead more people into the fields of particle physics, astronomy, and cosmology.

Historically, many different dark matter candidates have been introduced to explain the missing visible matter in the universe. These possible candidates range from dark baryonic matter to primordial black holes and it has even been proposed that the theory of gravity needs to be modified and that there is radically less dark matter than currently believed in the universe [1]. In time, though, the explanation has mostly settled on dark matter being elementary particles, and most likely one (or several) new elementary particle(s).

The candidates most recent studies have focused on are heavier candidates like WIMPs, with masses larger than approximately 50 GeV [2], but there is a wide range of possible candidates, such as light dark matter, with masses between 10^{-22} and 1 eV, or with masses being even lower. Any of these ranges for masses could hold a candidate (or several candidates) that is the best fit for the dark matter observed in and around our galaxy. Since there are several potential mass ranges for dark matter candidates and there has not been any breakthrough in the realm of heavy dark matter candidates it could be a good idea to focus on these lighter candidates for dark matter as well. In Section 1.1 the history of dark matter exploration is explained as well as the evidence for the existence of dark matter in general and a few different dark matter candidates in particular. The section finishes with a brief explanation of the poorly explored wave dark matter theory, which is the foundation for the dark matter candidate that is explored in this thesis.

There are three ways to search for dark matter candidates: direct detection, which can be a way to detect WIMPs, collider experiments to detect missing momentum and energy possibly corresponding to dark matter, and annihilation of dark matter particles which could result in detectable standard model particles [3]. In this thesis, a possible direct detection experiment that could be used to search for light dark matter particles at Chalmers University of Technology (CTH) is examined. The ex-

periment, and direct detection of dark matter in general, is explained in Section 1.2.

The focus in this thesis lies squarely on a dark matter candidate that is a wave dark matter vector boson. Because of the way this dark matter candidate interacts with matter and because of its light mass, it can be compared with the so called "dark photon" [4]. The theory for vector bosons laid out in [5] is used together with the statistical framework developed in [6] to find the experimental sensitivity for the proposed experiment meant to search for light dark matter previously mentioned. The thesis description is further expanded in Section 1.3. In Chapter 2 a more in-depth explanation of the vector wave dark matter candidate is given as well as a brief physical explanation of the connection between it and the dark photon. The statistical framework from [6] is presented in Chapter 3. Finally in Chapter 4 the resulting exclusion and discovery limits determining the experimental sensitivity for the proposed experiment are shown. These results are compared to the results presented in [5] and discussed.

1.1 Background

Dark matter is a type of matter that does not interact with the electromagnetic field or via the strong force, and as such it is difficult to measure, but it has been discovered to make up most of the total matter in the universe [1]. That dark matter exists at all, however, and how the dark matter would be described is not obvious. Historically it has taken time and effort for the theory of dark matter to be accepted and a satisfying description of dark matter is yet to materialize. In this section the history of and evidence for dark matter as well as the reasons for this thesis' focus on very light dark matter is discussed.

1.1.1 History

Humans have viewed the skies since before they formed settlements, but it was fairly recently that the telescope was invented which allowed a more scientific view of the sky [1]. Though it was not until the 20th century that the concept of dark matter could be formulated in a way that could be recognized today. However, the need for more mass that is not visible was discussed as early as the mid part of the 19th century, but then focusing on the possibility of invisible stars and dark clouds to describe the problems they encountered. The real first discussion of dark matter was therefore just the possibility of matter that was too dark to be seen. In the early part of the 20th century calculations of dynamics in the Milky Way by viewing the stars as gas particles indicated that the the majority of these "stars" could be dark [1]. This was done by comparing velocity dispersion for the stars with the size of the system. At this time though, it was commonly believed to be more than or at least similar amounts of visible matter to that of dark matter.

When the virial theorem was first applied on a galaxy cluster, the Coma Cluster, to find the mass of said cluster in the early 1930s it was found that the velocity dispersion from the visible matter should be about 80 km/s, but the measured velocity

dispersion was about 1000 km/s [1]. The person who first did this (Fritz Zwicky) thought that the "dark matter" was in "the form of cool and cold stars, macroscopic and microscopic solid bodies, and gases." Clearly the move to view dark matter as non-baryonic was still ways of. And indeed a lot of astronomers did not believe that the findings could be true as the invisible mass to visible mass ratio would be too great. Several alternative explanations were offered but they did not stand the test of time. During the 1970s, gas was ruled out as the main part of this dark matter and so different (and strange) solutions started to be discussed. For more information about these strange solutions that were proposed from this time and onwards, the reader is refered to [1]. The velocity dispersion of the galaxy cluster is also further discussed as evidence for dark matter in Section 1.1.2.1.

Another key element in the case for dark matter was the rotation curve of galaxies, i.e. the rotational velocity as a function of radial distance from the galaxy centre. These have been measured to be approximately constant and measurements of this nature have been made since the 1910s [1]. It was not until the 1970s, however, that scientists started to worry about the discrepancy between the observed mass and the observed rotational velocities at the the outer parts of the galaxies, as earlier optical observations could not find what can be found with radio observations. With the rotational velocity, the mass of the galaxy can be calculated and a mass to light ration can be inferred. Since the expected mass from the visible part of the galaxy was different from what was measured from rotational curves, scientists began to lean more in favor of the existence of dark matter as separate from ordinary visible matter. The rotation curve as evidence for dark matter is described in more detail in Section 1.1.2.2.

Though most other hypotheses of what could be this "dark matter" were discarded, the view that it might be made out of subatomic particles did not become the main focus for researchers until the later parts of the 1980s [1]. MACHOs (massive astrophysical compact halo objects, a baryonic alternative) were not disproven to be a dominating part of dark matter until the early part of the 21st century, but non-baryonic dark matter candidates were a leading model as early as the end of the 1980s. In the late 1970s the neutrino was proposed to be able to account for the missing mass, but by use of numerical simulations it was shown, in the 1980s, that the neutrino and similar particles could not be the dominating part of the dark matter mass.

Supersymmetry (a symmetry that relates bosons to fermions, predicting "new" particles) was invented in the 1970s [1]. It can be used to predict particles outside of the standard model that could be dark matter. And in the late part of the 1970s the axion, a particle that could solve the strong charge conjugation parity problem in quantum chromodynamics, was proposed. It is also a fitting dark matter candidate. Weakly interacting massive particles (WIMPs) was proposed as a dark matter candidate in the 1980s, but other possible candidates have been proposed as well, such as wave dark matter [7]. In more resent days this wave dark matter theory has been established and being such a new phenomenon it is not surprising that it is so poorly explored. Because of this it has not yet yielded any results that can be discussed in

the same way MACHOs and WIMPs can be discussed. Wave dark matter is briefly described in Section 1.1.3.4 and connected more clearly to this thesis in Chapter 2.

1.1.2 Evidence for dark matter

The evidence for dark matter presented here is in the same order as the corresponding discoveries in Section 1.1.1, and evidence not mentioned there are presented later in this section. The evidence does not only pertain to the *existence* of dark matter but also that it is most likely *non-baryonic*. The possibility of the theory of modified Newtonian dynamics (MOND) being correct is not discussed here but can be read about in [1].

1.1.2.1 Velocity dispersion for galaxy clusters

As described earlier, using the velocity dispersion of a galaxy to find the mass or vice versa using the virial theorem and not accounting for dark matter yields a contradiction [1]. The virial theorem states that

$$\langle T \rangle = -\frac{1}{2} \langle U \rangle , \tag{1.1}$$

where T is the kinetic energy of the system and U the gravitational potential of the system. If this is applied on the Coma Cluster, with the assumption that the mass of a galaxy is the measured mass before dark matter was taken into account, about 10^9 solar masses, the contradiction is found [8]. Taking the number of galaxies that had been measured at the time when Swicky did this calculation for the first time, 800 (now it is known to have over 1000 galaxies) so that the total mass of the Coma Cluster becomes $M_{\text{Coma}} = 1.6 \cdot 10^{42}$, with radius of the cluster being about $R \approx 10^{19}$ km, the theorem in (1.1) yields,

$$\frac{1}{2} \left\langle v^2 \right\rangle M_{\text{Coma}} = -\frac{1}{2} \frac{-3}{5} G \frac{M_{\text{Coma}}^2}{R}. \tag{1.2}$$

Here G is the gravitational constant, and from this expression the square root of the average velocity squared can be found:

$$\begin{aligned} \sqrt{\langle v^2 \rangle} = \sqrt{\frac{3}{5} G \frac{M_{\text{Coma}}}{R}} &\approx \sqrt{\frac{3}{5} \cdot 6.67 \cdot 1.6 \cdot 10^{-20} \cdot 10^{42} \cdot 10^{-19} \text{ km}^2/\text{s}^2} \\ &\approx 80 \text{ km/s}. \end{aligned} \tag{1.3}$$

But the average measured velocity is about 1000 km/s and thus there is a contradiction. But this does not *prove* that there is a missing mass or that the mass is dark matter. It could be argued that the Coma Cluster and other clusters this is applied to are not stable enough for the virial theorem. However it can be shown that the age of the clusters would have to be lesser than the age of the galaxies in them if that was true [1].

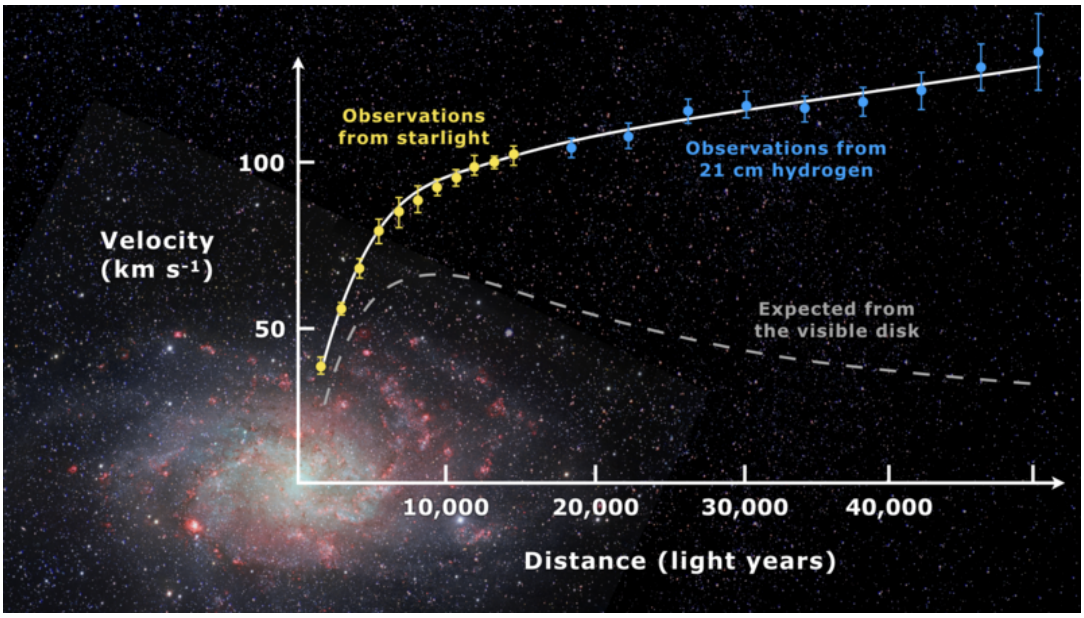

Figure 1.1: Two rotation curves overlayed on the image of a galaxy (Messier 33). The observed rotation curve based on the measured (yellow and blue) data shows a higher rotational velocity than the expected rotation curve. At radii outside of the galactic centre the velocity decreases for the expected rotation curve, while the velocity for the observed curve increases slightly. Credit: Mario De Leo, CC BY-SA 4.0 `https://creativecommons.org/licenses/by-sa/4.0`, via Wikimedia Commons, `https://upload.wikimedia.org/wikipedia/commons/c/cd/Rotation_curve_of_spiral_galaxy_Messier_33_%28Triangulum%29.png`.

1.1.2.2 Rotation curves of galaxies

To find out more about the unseen matter surrounding galaxies one can observe the galaxies, and find discrepancies between the observed mass and the velocity of the galaxy [1]. The rotation curve of a (spiral) galaxy is measured both in the optical and radio ranges since the outer edges of the galaxy has no stars but rather a lot of hydrogen gas. These measurements are used to find the rotational velocity as a function of the distance from the galactic centre. The expected rotation curve calculated from only visible mass would first increase in the central region and then decrease with increased radius (the increase would be roughly $v \propto r$ and the decrease $v \propto r^{-1/2}$) [9]. When the rotational velocity is actually measured, however, the rotational velocity continues to increase and becomes approximately constant at the outer edges [1]. This discrepancy can be seen in Figure 1.1, which shows the expected rotation curve and the actual observed rotation curve of a spiral galaxy (Messier 33). From this discrepancy, the conclusion can be drawn that there is some sort of missing matter that explains why the observed rotation curve does not decrease with radius. Since the rotational velocity is approximately constant far "outside" the galaxy, this also provides evidence for the existence of what we now call a dark matter halo, that additionally has a different distribution than the visible matter. However to show that dark matter is unlikely to be baryonic matter, more evidence needs to be discussed.

1.1.2.3 Lack of evidence for baryonic dark matter

The most obvious candidate for dark baryonic matter would be gas [1], but the gas surrounding galaxies can be shown to correspond to less than 2% of the missing matter. This is done by observing X-ray emissions from the ionized gas. Other methods to find baryonic dark matter have similarly come up lacking, for example the use of gravitational microlensing to find MACHOs have yielded results that indicate a very low amount of MACHOs [10]. Gravitational microlensing is a method where a small massive object (with mass between the mass of a planet to that of a star), bends the light from a source behind it in relation to the observer, so that the observer sees several versions of the source. In [10] the EROS-2 Collaboration used this to find existing MACHOs, but with few observations their results indicate that MACHOs make up less then 8 % of the missing matter in the dark matter halo. Thus it is highly unlikely that the dark matter in the galactic halo is either gas or MACHOs.

In general though, the evidence against baryonic dark matter comes mainly from observed the baryon density of the universe. The Planck Collaboration [11] has calculated the baryon density [1] and found it to be about $\Omega_b \approx 0.02225$. With such a small density (it corresponds to baryonic matter being about 7% of the total matter) it is highly unlikely that baryonic matter makes up anything more than a very small amount of the unseen dark matter.

1.1.3 Non-baryonic dark matter candidates

While baryonic dark matter have been mostly excluded, there are several non-baryonic dark matter candidates that have been suggested. This thesis focuses on very light candidates, since there exists experimental possibilities at CTH to make potential discovery in this field and heavy candidates have been thoroughly explored already. In this section a few candidates are discussed to showcase the issue regarding these as candidates, starting with the lighter neutrino and the axion and then moving on to the heavier WIMPs. But first a quick discussion about hot and cold dark matter, and thermal as well as non-thermal creation of dark matter particles.

Hot dark matter candidates are candidates that would have been relativistic during structure formation while cold dark matter candidates would have been non-relativistic [1]. If the dominating dark matter in the universe was hot this would have lead to larger dark matter structures forming first and then fragment to smaller (i.e. galaxy sized) structures later. Cold dark matter, in contrast, would have formed smaller halos first and then merging would have lead to bigger structures. Simulations of dark matter structures have shown that dark matter was most likely cold, resulting in hot dark matter seemingly being a poor match for being the dominating part of the dark matter in the universe.

If dark matter was thermally created it was created during the thermodynamical equilibrium when the universe was young [12]. Eventually the dark matter would have stopped being in this equilibrium as the universe cooled, and thus the particle

would no longer be created. However thermally created dark matter candidates cannot be to light if they are going to be an example of cold dark matter since the particles would have had to freeze-out of the thermal equilibrium in the early universe [1]. Non-thermally created dark matter particles, however, can be light without being hot. These particles are created at low enough temperatures so that they do not reach thermal equilibrium or have a weak enough interaction with the thermal plasma so that they cannot be seen as coupled to it [13]. As such, non-thermally created dark matter offers the possibility of cold light dark matter, important for structure formation.

1.1.3.1 Neutrinos

One of the earliest candidates for dark matter was the neutrino [1]. Since it is stable and do not interact through either the electromagnetic force nor the strong force it is an interesting candidate as this fits well with observations of how dark matter should interact (at most weakly). However because of their low mass and how they were created (thermally) it is an example of a hot dark matter candidate and because of this it is not seen as a viable candidate for the dominating part of the dark matter in the universe anymore. As such, the neutrino as dark matter cannot account for the measured dark matter.

1.1.3.2 Axions

The axion were first thought of to solve the strong charge conjugation parity problem in quantum chromodynamics, but is also an excellent dark matter candidate [1]. It is weakly interacting and has a low mass ($\lesssim 10^{-3}$ eV) and can be created both non-thermally. As such it can be an example of cold dark matter, and light axions with masses between 10^{-6} eV and 10^{-4} eV could describe all the dark matter measured. Measuring the axion could be done in the same way as the vector boson in focus in this article, with use of direct detection experiments. It can be noted that the axion can be explored as a wave dark matter candidate [4].

1.1.3.3 WIMPs

A possible set of candidates of cold dark matter are WIMPs, which are weakly interacting which is a desired type of interaction for dark matter [1]. They are heavy (with a mass in the GeV-TeV-scale) and as such could be a thermal relic and yet be cold dark matter. Notably WIMPs could make up all measured dark matter in the universe. However searches for WIMPs should have yielded results by now. They should not be too difficult to find, and as such the particles may very well not exist, or be in a higher mass range than initially thought [2].

1.1.3.4 Wave dark matter

A poorly explored theory of dark matter is the wave dark matter theory [7]. It states that light enough dark matter candidate can be described as classical waves. It should be noted that because of the Pauli exclusion principle the particles are bosonic. The theory has some interesting implications. On small scales the dark

matter has a wave-like behaviour, but it retains the cold dark matter behaviour on larger scales.

An example of a wave dark matter candidate is the previously mentioned axion, as it is light enough. Another is the particle in focus of this thesis, the vector boson which has a peculiar interaction that is not one of the four fundamental interactions. It interacts with the baryon number minus the lepton number [4]. The vector dark matter field yields an equivalence principle (EP) violating force and if it is tested on a charge-neutral test object it only interacts with the neutron number meaning that tests on this candidate would be fairly easy to perform.

1.2 Direct detection

A wave dark matter candidate could hypothetically be measured with direct detection experiments. These experiments require the measuring of the direct effect of the dark matter on a sensor of some kind [3]. More massive dark matter particles, like the WIMP, can cause a noticeable recoil of the nucleus in matter, but when it comes to lighter dark matter candidates such an recoil would be undetectable, so electron recoils are often searched for instead. However, in the case of wave dark matter, which is a wave rather than individual particles, nuclear recoils could be detected. The wave nature of the dark matter makes detection more easy as the whole test object would fit inside of the dark matter wave, causing a potentially noticeable force on the object from the totality of particles in said wave, depending on the coupling constant for the dark matter candidate in question. A realistic wavelength in wave dark matter is between about 10000000 km (for a dark matter candidate with the mass $1.24 \cdot 10^{-13}$ eV) and about 300000 km (for a dark matter candidate with the mass $4.14 \cdot 10^{-12}$ eV) as can be seen in Chapter 2, while the test objects assumed in this thesis has a radius of 1 µm and 100 µm.

At Chalmers University of Technology there is a group that could do a fitting direct detection experiment for the vector boson wave dark matter candidate (specifically at the Quantum Technology Laboratory which operates at MC2) [14]. The experimental set-up is described in detail in [15]. A microscopic superconductive object made out of lead is levitated in a magnetic trap produced by two superconducting coils. The test object levitates near the minimum of the magnetic field. When the particle is moved (for instance by a dark matter induced acceleration) it changes the magnetic flux threading the loops so that the current inside those loops changes. A dc-SQUID magnetometer is connected to the loops and converts the flux to voltage, which is measured.

In this experiment, the background noise affecting the test object is assumed to be thermal and to have an acceleration power spectral density (PSD) based on the size of the test object as well as based on the mechanical quality factor $Q_{\mathrm{m}} = \omega_{\mathrm{t}}/\gamma_{\mathrm{m}}$. Here γ_{m} is the dissipation and $\omega_{\mathrm{t}}/2\pi$ is the trap frequency of the experiment. The background PSD (in terms of acceleration squared per hertz) is for a test object with the temperature, T, the Boltzmann constant, k_B, and the mass of the test

object, $m_{\text{t.o}}$,

$$\lambda_{\text{B}} = \frac{4k_B T \gamma_{\text{m}}}{m_{\text{t.o}}}. \tag{1.4}$$

For a test object with radius 1 µm, and a conservative value of the mechanical quality factor 10^7 and an optimistic value 10^{11}, the background is $7 \cdot 10^{-16}$ and $7 \cdot 10^{-20}$, respectively. For a test object with radius 100 µm, and a conservative value of the mechanical quality factor 10^7 and an optimistic value 10^{11}, the background is instead $7 \cdot 10^{-22}$ and $7 \cdot 10^{-26}$, respectively. These background values are used later in the thesis.

1.3 Thesis

Since the searches for dark matter currently in focus have yielded little results it would be a good idea to focus more on different types of dark matter candidates. As such the goal of this thesis is to find the potential experimental sensitivity of the experiment discussed in Section 1.2 for a wave dark matter candidate. The particle in focus is as discussed in the previous section a vector boson. The goal is to find the exclusion limit and the discovery limit for the coupling constant between a charge-neutral test object and the dark matter field and plot it against a realistic mass interval based on the mass interval used in [6] to simplify comparisons. First the acceleration on a test object induced by a vector dark matter wave is calculated, inspired by [5]. Using this acceleration and a likelihood formalism developed in [6], the exclusion and discovery limits can be calculated for this potential experiment.

However it should be noted that just because a candidate have not be found yet does not mean that it does not exist. This thesis does not state that searches into heavier candidates is fruitless, merely that other searches should be of greater focus. Note that throughout this article natural units are used, i.e. the speed of light, $c := 1$, and the reduced Planck constant, $\hbar := 1$.

2

The dark matter model

In this chapter necessary theoretical knowledge surrounding the dark matter (DM) candidate discussed in this thesis is given, as well as a derivation of the measurable acceleration said particle can apply on a test object in the potential experiment at CTH. This chapter follows the derivation done in [5] for the vector boson and was suggested for experimentation in [4]. Section 2.1 discusses the theory of wave dark matter and what is assumed when using this as a framework. Some information about the vector boson regarded in this article is presented in Section 2.2. Finally the derivation of the acceleration from one dark matter wave on a charge-neutral sensor is derived in full in Section 2.3.

2.1 Wave dark matter

The term "wave dark matter" describes dark matter particles that are very light, so light that describing them as a classical wave is a good approximation [7]. Such a field has the property of having an angular frequency,

$$\omega = \sqrt{m_{\mathrm{DM}}^2 + m_{\mathrm{DM}}^2 v^2} = m_{\mathrm{DM}}\sqrt{1+v^2} \approx m_{\mathrm{DM}}\left(1 + \frac{v^2}{2}\right), \tag{2.1}$$

which for realistic velocities can be approximated to $\omega \approx m_{\mathrm{DM}}$, for a dark matter particle with the mass m_{DM} and speed v. For particles to be able to be described in such a way they have to have a high enough occupancy within their de Broglie volume. The de Brogile volume is

$$\lambda_{\mathrm{dB}}^3 = \frac{8\pi^3}{m_{\mathrm{DM}}^3 v^3}, \tag{2.2}$$

and the occupancy number within this volume is the local density of the particles divided by their mass and multiplied by the volume,

$$\rho\frac{\lambda_{\mathrm{dB}}^3}{m} = \rho_{\mathrm{DM}}\frac{8\pi^3}{m_{\mathrm{DM}}^4 v^3}, \tag{2.3}$$

which for small masses is huge. To find out what mass range such particles could be within, a realistic value of the dark matter density and of the velocity of the

dark matter particles have to be found. The local dark matter density is typically estimated to be between 0.3 and 0.4 GeV/cm^3 [16]. In this article the value 0.4 GeV/cm^3 is used like in [6] but the final results are easily modified for any other value of the density. The velocity dispersion for dark matter can be estimated to be about 10^{-3} in the bulk of the halo [4]. This yields an estimated occupancy number of about $(29.6\text{ eV})^4/m_{\text{DM}}^4$. So for a dark matter particle with a mass lower than about 30 eV the de Broglie volume would contain several particles. If the mass is much lower the volume would contain enough particles so that the particle could be well described by a classical wave.

The smallest mass possible for this approximation needs to be discussed as well. Even an extremely tiny mass would have an associated wave, but an easy thought-experiment shows that the de Brogile wavelength would be larger than the diameter of the observable universe (about 28.5 Gpc) if the mass is less than about $1.4 \cdot 10^{-30}$ eV. However the model breaks down for far more massive particles. If, for instance, the wave length is larger than the diameter of a small dwarf galaxy's halo where dark matter has been measured then the approximation breaks down since there would not be enough particles in the halo for the classical wave approximation to fit said observations [17]. To then find a realistic minimum value for the mass of the dark matter the de Brogile wavelength is set to be lower than 0.1 kpc:

$$0.1\text{ kpc} > 10^3 \cdot \frac{1\text{ eV}}{m_{\min}} \cdot h \cdot c \approx \frac{4 \cdot 10^{-22}\text{ eV}}{m_{\min}} 0.1\text{ kpc}. \tag{2.4}$$

The smallest possible mass is then seen to be about 10^{-22} eV, depending on the velocity of the dark matter particle. In this article the masses regarded are between 1 eV and 10^{-22} eV, meaning that the particle can be described by a classically wave without having an unphysically large de Broglie wavelength.

2.2 The vector boson

In Chapter 1 the vector boson this thesis focuses on is introduced, but here some motivation for this choice is given. The particle has to be a boson since fermions are a bad fit with the wave dark matter model [7]. Because fermions are governed by the Pauli exclusion principle, it excludes the possibility that fermions have a high occupancy number which is a necessary condition for the wave dark matter approximation. Moreover, the spin and the Lagrangian of this boson need to be specified. In this article the spin-1 boson with the interaction part of the Lagrangian being $gA_\mu\bar{\psi}\gamma^\mu\psi$, where g is the coupling constant, ψ is a fermion, A_μ is the vector field, and γ^μ is a gamma matrix, is focused on [4]. Specifically, the focus is on how this field interacts with *only* neutrons, since the field couples to the baryon number minus the lepton number (see eq. 2.5), giving an easier interaction in case of a charge-neutral sensor.

Furthermore this means that the force from dark matter upon a test object is EP-violating, meaning that experiments can be optimized more greatly since (in this

case) the number of neutrons can be different for different charge-neutral test objects [4]. Using this, the force can be measured on different test objects, since the EP-violating force leads to different accelerations of the objects that does not correlate to the difference in mass for said test objects. As such the effect from the dark matter wave can be measured even if there is an additional effect from the physical displacement of the test objects. Note also that the force is time-dependent and not static, meaning that systematic effects do not mimic the effect from the dark matter wave, the "signal," since the force is oscillating at the frequency of the dark matter mass.

This vector boson and scalar boson are two candidates suggested for further research in [4] and as such are interesting to apply the statistical framework seen in [6] to. In this thesis the focus is on the vector boson, but in [5] both candidates are discussed, both only with coupling to the neutron to ease comparison between the two candidates, albeit not using the same statistical framework as this thesis.

2.3 Effect on a charge-neutral test object

To find the effect on a charge-neutral test object from dark matter the equation of motion for the test object first needs to be derived. In this case finding the equations of motion for the centre of mass of the test object can be done through the Lagrangian of a neutron in the test object. The force upon the neutron needs only be multiplied with the number of neutrons in the test object to yield the force on the test object. The Lagrangian is simple, the only difficulty is finding the potential resulting from the dark matter wave, which is done in the next subsection.

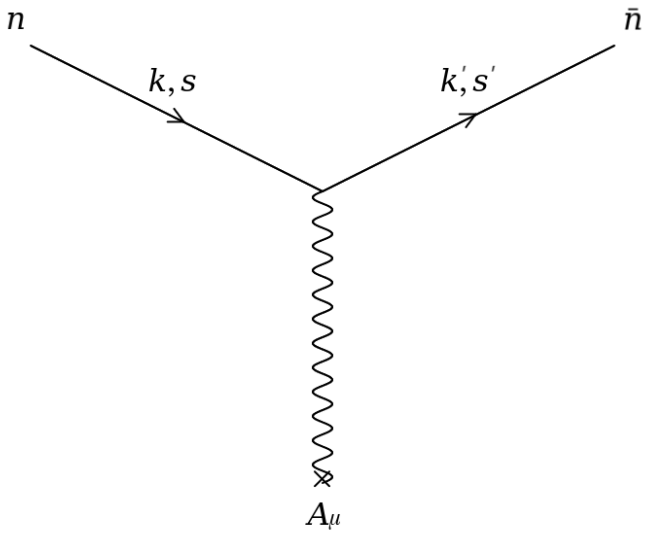

Figure 2.1: Feynman diagram for neutrons scattering against an external vector bosonic field. The incoming neutron is labeled with n and has momentum k and spin s while the outgoing neutron (or incoming anti-neutron), labeled $\bar{n}$, has momentum k' and spin s'. The cross symbolises that the dark matter, A_μ, is an external source.

2.3.1 The potential from the dark matter field

The potential experienced by a neutron interacting with the dark matter field can be found from the Born approximation and time-dependent perturbation theory used on the scattering matrix (S-matrix). The interaction term between the vector field A_μ and the neutron n is the third term of the following Lagrangian, given in [5]:

$$\mathcal{L} = -\frac{1}{4}F_{\mu\nu}F^{\mu\nu} - \frac{1}{2}m_{\mathrm{DM}}^2 A_\mu A^\mu + gA_\mu \bar{n}\gamma^\mu n. \tag{2.5}$$

From this Lagrangian an S-matrix for the interaction between neutron and the dark matter filed can be found. Since the dark matter behaves like a classical wave the interaction is best described as neutrons scattering against an external dark matter field [18]. In Figure 2.1 the Feynman diagram for the neutrons scattering against an external vector bosonic field is shown.

The first order S-matrix from quantum field theory (QFT) is:

$$\begin{aligned} S_{fi}^{(1),QFT} &= -ig\int d^4x \langle \overbrace{f| - A_\mu(x)\bar{n}}\gamma^\mu \overbrace{n|i}\rangle \\ &= ig\int d^4x A_\mu(x)\langle \overbrace{f|\bar{n}}\gamma^\mu \overbrace{n|i}\rangle \\ &= ig\int d^4x A_\mu(x)\bar{u}^{s'}(k')\gamma^\mu u^s(k)e^{i[k'-k]\cdot x}\langle 0|0\rangle, \end{aligned} \tag{2.6}$$

where Wick contractions are used, $\langle f|$ and $|i\rangle$ represents the final and the initial states of the anti-neutron and the neutron, and the last step requires usage of the Feynman rules. The non-relativistic spin-sum rules are [19]:

$$\bar{u}^{s'}(k')\gamma^\mu u^s(k) \approx \left(2m_{\mathrm{n}}, \left[\vec{k'} + \vec{k}\right]\delta^{s's} - 2i\left[\vec{k'} - \vec{k}\right] \times \vec{s}\right) \tag{2.7}$$

leading to:

$$\begin{aligned} S_{fi}^{(1),QFT} &= ig\int A_\mu(x)\bar{u}^{s'}(k')\gamma^\mu u^s(k)e^{i[k'-k]\cdot x}d^4x = ig\tilde{A}_\mu(k'-k)\bar{u}^{s'}(k')\gamma^\mu u^s(k) = \\ &= \left[q = k' - k\right] \approx ig\left\{2m_{\mathrm{n}}\tilde{A}_0(q)\delta^{s's} - \vec{\tilde{A}}(q)\cdot\left[(\vec{k'} + \vec{k})\delta^{s's} - 2i\vec{q}\times\vec{s}\right]\right\} = \\ &= \left[s = \frac{1}{2}\vec{\sigma}^{s's}\right] = ig\left\{2m_{\mathrm{n}}\tilde{A}_0(q)\delta^{s's} - \vec{\tilde{A}}(q)\cdot\left[(\vec{k'} + \vec{k})\delta^{s's} - i\vec{q}\times\vec{\sigma}^{s's}\right]\right\} \\ &= ig\left\{\left[2m_{\mathrm{n}}\tilde{A}_0(q) - \vec{q}\cdot\vec{\tilde{A}}(q) - 2\vec{k}\cdot\vec{\tilde{A}}(q)\right]\delta^{s's} - i\left[\vec{q}\times\vec{\tilde{A}}(q)\right]\cdot\vec{\sigma}^{s's}\right\}. \end{aligned} \tag{2.8}$$

In the last step, the anti commutativity and the circular-shift property of the cross product was used as well as that $k' + k = q + 2k$. For this result to lead to the potential experienced by the charge-neutral test object the Born approximation together with time-dependent perturbation theory has to be used [20, 21]. But for the Born approximation to work the S-matrix has to be compared with an S-matrix derived from non-relativistic quantum mechanics. The difference from the S-matrix derived through quantum field theory is a factor $2m_n$ since this term comes from the relativistic normalization of the ground state. Finally the spin of the neutrons has

to be dealt with. Since the neutrons in the test object are generally unpolarized, it can be assumed that $s' = s$. This leads to $\delta^{s's} = 1$ and that $\vec{\sigma}^{s's} = 0$ since Pauli-matrices are traceless. The Born approximation can now be used to find the quantum mechanical (QM) S-matrix:

$$S_{fi}^{(1),QM} = -i\tilde{V}(q). \tag{2.9}$$

Here $\tilde{V}$ is the Fourier transformed potential experienced by the test object. Comparing with the S-matrix from QFT, the Fourier transform of the potential can be explicitly found:

$$\tilde{V}(q) = -g\Big\{\tilde{A}_0(q) - \frac{1}{2m_\mathrm{n}}\vec{q}\cdot\vec{\tilde{A}}(q) - \frac{1}{m_\mathrm{n}}\vec{k}\cdot\vec{\tilde{A}}(q)\Big\}. \tag{2.10}$$

Inverse transforming, the potential experienced by the neutron becomes:

$$\begin{aligned} V(x) &= -g\Big\{A_0(x) - \frac{i}{2m_\mathrm{n}}\vec{\nabla}\cdot\vec{A}(x) - \frac{\vec{k}\cdot\vec{A}(x)}{m_\mathrm{n}}\Big\} = \\ &= -g\Big\{A_0(x) - \frac{i}{2m_\mathrm{n}}\vec{\nabla}\cdot\vec{A}(x) - \vec{v}_\mathrm{n}\cdot\vec{A}(x)\Big\}. \end{aligned} \tag{2.11}$$

This can be further simplified since

$$\vec{\nabla}\cdot\vec{A}(x) = 0 \tag{2.12}$$

in the coulomb gauge, leading to a final expression for the potential:

$$V(x) = -g\Big\{A_0(x) - \vec{v}_\mathrm{n}\cdot\vec{A}(x)\Big\}. \tag{2.13}$$

2.3.2 The acceleration from the dark matter field

To find the acceleration experienced by the test object in this potential the Lagrangian for one of the neutrons in it can be examined:

$$\mathcal{L} = \frac{1}{2}m_\mathrm{n}|\dot{\vec{x}}|^2 - V(t,\vec{x},\dot{\vec{x}}). \tag{2.14}$$

By applying the Euler-Lagrange equation:

$$0 = \frac{\partial\mathcal{L}}{\partial\vec{x}} - \frac{d}{dt}\frac{\partial\mathcal{L}}{\partial\dot{\vec{x}}} \implies m_\mathrm{n}\ddot{\vec{x}} = \frac{d}{dt}\frac{\partial V}{\partial\dot{\vec{x}}} - \frac{\partial V}{\partial\vec{x}}, \tag{2.15}$$

the equations of motion can be found. With the potential from eq. (2.11):

$$\frac{d}{dt}\frac{\partial V}{\partial\dot{\vec{x}}} = g\Big\{\frac{\partial\vec{A}(x)}{\partial t} + \big[\vec{v}_\mathrm{n}\cdot\vec{\nabla}\big]\vec{A}(x)\Big\} \tag{2.16}$$

$$-\frac{\partial V}{\partial\vec{x}} = g\Big\{\vec{\nabla}A_0(x) - \vec{\nabla}\big[\vec{v}_\mathrm{n}\cdot\vec{A}(x)\big]\Big\}, \tag{2.17}$$

the force on the neutron from the vector field, given by $m_{\mathrm{n}}\ddot{\vec{x}}$, becomes:

$$\vec{F} = -g\Big\{-\frac{\partial \vec{A}(x)}{\partial t} - \vec{\nabla}A_0(x) + \vec{\nabla}\big[\vec{v}_{\mathrm{n}} \cdot \vec{A}(x)\big] - \vec{A}(x)\big[\vec{v}_{\mathrm{n}} \cdot \vec{\nabla}\big]\Big\}. \tag{2.18}$$

Using the identity for the triple product,

$$\vec{a} \times \big(\vec{b} \times \vec{c}\big) = \vec{b}\big(\vec{a} \cdot \vec{c}\big) - \vec{c}\big(\vec{a} \cdot \vec{b}\big), \tag{2.19}$$

the force is simplified to look like a Lorentz force, but for dark matter coupled to the neutron:

$$\begin{aligned}\vec{F}(x) &= -g\Big\{-\frac{\partial \vec{A}(x)}{\partial t} - \vec{\nabla}A_0(x) + \vec{v}_{\mathrm{n}} \times \big[\vec{\nabla} \times \vec{A}(x)\big]\Big\} \\ &= -g\Big\{\vec{E}_{\mathrm{DM}}(x) + \vec{v}_{\mathrm{n}} \times \vec{B}_{\mathrm{DM}}(x)\Big\},\end{aligned} \tag{2.20}$$

with $\vec{E}_{\mathrm{DM}}(x) = -\frac{\partial \vec{A}(x)}{\partial t} - \vec{\nabla}A_0(x)$ and $\vec{B}_{\mathrm{DM}}(x) = \vec{\nabla} \times \vec{A}(x)$. The similarities to a photon are quite clear from this, as this expression has the same form as the Lorentz force for the actual photon.

Focusing on eq. (2.20) and using the Lorenz gauge ($\partial^\mu A_\mu = 0$ implying that $A_0 = \vec{v} \cdot \vec{A}(x)$) results in:

$$\vec{F}(x) \approx g\frac{\partial \vec{A}(x)}{\partial t}. \tag{2.21}$$

Since the dark matter velocity is very small $A_0(x)$ is much smaller than the absolute value of $\vec{A}(x)$. A Fourier transform of $\frac{\partial \vec{A}(x)}{\partial t}$ is much greater than the Fourier transform of $\vec{v}_{\mathrm{n}} \times \big[\vec{\nabla} \times \vec{A}(x)\big]$ so that the last term also can be neglected by the same argument.

In order to find the acceleration on a neutron in the test object, an expression for the vector field needs to be found. For a free vector field the Klein-Gordon equation is the equation of motion. Since $A_0(x) << \vec{A}(x) = A^i(x)$, one needs only look at the spatial coordinates:

$$(\Box + m_\phi^2)A^i(x) = 0, \tag{2.22}$$

with solution that A^i is best described as a plane wave. If C_{i1} and C_{i2} are constants and $C_{i1} + C_{i2} = C_i$, with eq. (2.21) the vector field is described as:

$$\begin{aligned}A_i(x) &= C_{i1}e^{i\left(\omega t - \vec{k}\cdot\vec{x}\right)} + C_{i2}e^{-i\left(\omega t - \vec{k}\cdot\vec{x}\right)} = \\ &= C_{i1}\left[\cos\left(\omega t - \vec{k}\cdot\vec{x}\right) + i\sin\left(\omega t - \vec{k}\cdot\vec{x}\right)\right] + \\ &+ C_{i2}\left[\cos\left(\omega t - \vec{k}\cdot\vec{x}\right) - i\sin\left(\omega t - \vec{k}\cdot\vec{x}\right)\right] = \\ &= [A_i \text{ real } \implies C_{i1} = C_{i2}] = C_i\cos\left(\omega t - \vec{k}\cdot\vec{x}\right).\end{aligned} \tag{2.23}$$

The relation between the density and the amplitude of the plane wave is known [22]:

$$\rho_{\mathrm{DM}} = \frac{1}{2}\omega^2|C_i|^2, \tag{2.24}$$

leading to the amplitude being expressed as:

$$\left|\vec{C}\right| = \frac{\sqrt{2\rho_{\mathrm{DM}}}}{\omega}. \tag{2.25}$$

Finally this yields an expression for the absolute value of the force on one neutron:

$$|\vec{F}(x)| = F(x) = \left| g\frac{\partial}{\partial t}\vec{A}(x) \right| = g\sqrt{2\rho_{\mathrm{DM}}}\sin\left(\omega t - \vec{k}\cdot\vec{x}\right) \tag{2.26}$$

Note that the direction of this force in relation to the dark matter velocity is unknown in this expression. The absolute value of the acceleration of the charge-neutral test object is found by first multiplying it with the number of neutrons in the test object, and then dividing the force with the mass of the object. The mass of the test object can be approximated as the number of protons plus the number of neutrons times the mass of the neutrons. Defining

$$x_{\mathrm{t.o}} = 1 + \frac{N_{\mathrm{p}}}{N_{\mathrm{n}}} \tag{2.27}$$

as an experiment-dependent constant describing the relation between the number of protons to the number of neutrons, then

$$m_{\mathrm{t.o}} \approx m_{\mathrm{n}}\left(N_{\mathrm{n}} + N_{\mathrm{p}}\right) = x_{\mathrm{t.o}} N_{\mathrm{n}} m_{\mathrm{n}}, \tag{2.28}$$

where $m_{\mathrm{t.o}}$ is the mass of the test object. The acceleration of the test object then becomes:

$$a(x) = \frac{\sqrt{2\rho_{\mathrm{DM}}}}{x_{\mathrm{t.o}} m_{\mathrm{n}}} g \sin\left(\omega t - \vec{k}\cdot\vec{x}\right). \tag{2.29}$$

The $\vec{x}$ dependence can be approximated away since the displacement from the force on the test object is much smaller than the wavelength of the dark matter wave. Introducing a random phase yields the final expression for the acceleration:

$$a(t) = \frac{\sqrt{2\rho_{\mathrm{DM}}}}{x_{\mathrm{t.o}} m_{\mathrm{n}}} g \sin\left(\omega t + \phi\right). \tag{2.30}$$

3

Statistical framework

This chapter delves into a statistical framework developed in [6], which uses a likelihood function-based formalism to analyze experimental possibilities of measuring a light dark matter axion particle. In this thesis the framework is used for the vector boson to derive a likelihood function in Section 3.1 that has the acceleration from eq. (2.30) in Chapter 2 as input to replace actual experimental data. To mimic realistic experimental data, the velocity and phase of the fields representing individual dark matter particles are set to be different from one another, with the velocity following the velocity distribution from the Standard Halo Model (SHM). Using this theoretical acceleration, a power spectral density (PSD) can be derived and used as data in the likelihood. Additionally, a background is assumed to be present in the experiment, with its effect being mainly thermal effects on the experiment.

In Section 3.2 the derived likelihood is used to define two test statistics that can be used set limits on the experimental sensitivity of an eventual experiment. These test statistics specifically set limits on the coupling constant. One such limit is the exclusion limit which is the highest value that the coupling constant can be measured to have in order for the background to be the sole measurable contribution on the test object for the experiment. The exclusion limit was calculated at a 95% confidence level. The other is the discovery limit which is the lowest value the coupling constant need to have in order to claim discovery of a signal of dark matter for teh experiment. In this case the discovery limit was calculated at a level of 5σ.

3.1 The likelihood function

The likelihood function, $\mathcal{L}$, test a model, $\mathcal{M}$, containing a signal of dark matter plus background. To find this likelihood, the PSD of the acceleration first needs to be derived from the previously calculated acceleration [6]. To find it, the acceleration is rewritten as the sum of every contribution to the acceleration from each dark matter field representing individual particles with a random phase and an unknown velocity that follows the velocity distribution from the SHM.

A single dark matter, i, corresponding to a single particle among a total number of dark matter particles N_{DM} in the local region has an acceleration $a_i(t)$ on the

charge-neutral test object:

$$a_i(t) = g\frac{\sqrt{2\rho_{\mathrm{DM}}/N_{\mathrm{DM}}}}{x_{\mathrm{t.o}}m_{\mathrm{n}}}\sin\left[m_{\mathrm{DM}}\left(1+\frac{v_j^2}{2}\right)t+\phi_i\right]. \tag{3.1}$$

A set, Ω_j, is constructed for each particle with a velocity v_j. The velocities for the particles belonging to this set lie between v_j and $v_j + \Delta v$, with Δv so small that all velocities can be approximated to v_j, and the number of dark matter particles belonging to the set is N^j_{DM}. Using this, one can sum over i to find the contribution to the total acceleration from only the particles with a velocity of v_j:

$$\begin{aligned} a_j(t) &= g\sum_{i\in\Omega_j}\frac{\sqrt{2\rho_{\mathrm{DM}}/N_{\mathrm{DM}}}}{x_{\mathrm{t.o}}m_{\mathrm{n}}}\sin\left[m_{\mathrm{DM}}\left(1+\frac{v_j^2}{2}\right)t+\phi_i\right] = \\ &= g\frac{\sqrt{2\rho_{\mathrm{DM}}/N_{\mathrm{DM}}}}{x_{\mathrm{t.o}}m_{\mathrm{n}}}\cdot\Im\left\{\exp\left[im_{\mathrm{DM}}\left(1+\frac{v_j^2}{2}\right)t\right]\sum_{i\in\Omega_j}e^{i\phi_i}\right\}. \end{aligned} \tag{3.2}$$

To simplify this expression, a relation for the sum over phases can be used. To do this it is necessary to introduce a Rayleigh distributed random variable, α_j [23]:

$$P\big(\alpha_j\big) = \frac{2\alpha_j}{N^j_{\mathrm{DM}}}e^{-\alpha_j^2/N^j_{\mathrm{DM}}}. \tag{3.3}$$

Note that when the acceleration is summed over j, a random variable needs to be drawn for every j. Now taking the random variable and scaling by $\sqrt{N^j_{\mathrm{DM}}/2}$ simplifies the distribution so that

$$P\big(\alpha_j\big) = \alpha_j e^{-\alpha_j^2/2}, \tag{3.4}$$

leading to

$$\sum_{i\in\Omega_j}e^{i\phi_i} = \alpha_j\sqrt{N^j_{\mathrm{DM}}/2}\cdot e^{i\phi_j}. \tag{3.5}$$

The acceleration then becomes

$$a_j(t) = g\alpha_j\frac{\sqrt{\rho_{\mathrm{DM}}\cdot N^j_{\mathrm{DM}}/N_{\mathrm{DM}}}}{x_{\mathrm{t.o}}m_{\mathrm{n}}}\cdot\sin\left[m_{\mathrm{DM}}\left(1+\frac{v_j^2}{2}\right)t+\phi_j\right]. \tag{3.6}$$

The velocity of the local dark matter follows a distribution from the SHM [6]:

$$f_{\mathrm{SHM}}(v) = \frac{v}{\sqrt{\pi}v_0v_{\mathrm{obs}}}e^{-(v+v_{\mathrm{obs}})^2/v_0^2}\cdot(e^{4vv_{\mathrm{obs}}/v_0^2}-1), \tag{3.7}$$

with the the speed of the Sun relative to the halo rest frame, $v_{\mathrm{obs}}(\approx 232$ km/s), and the speed of the local rotation curve, $v_0(\approx 220$ km/s). Using this, one can find that

the amount of dark matter particles within Ω_j is $N^j_{\rm DM} = N_{\rm DM} f_{\rm SHM}(v_j)\Delta v$. This results in the total acceleration becoming:

$$\begin{aligned} a(t) &= g\sum_j \alpha_j \frac{\sqrt{\rho_{\rm DM}\cdot f_{\rm SHM}(v_j)\Delta v}}{x_{\rm t.o} m_{\rm n}} \cdot \sin\left[m_{\rm DM}\left(1+\frac{v_j^2}{2}\right)t+\phi_j\right] \\ &= \sqrt{A}\sum_j \alpha_j \sqrt{f_{\rm SHM}(v_j)\Delta v}\cdot \sin\left[m_{\rm DM}\left(1+\frac{v_j^2}{2}\right)t+\phi_j\right] \end{aligned} \tag{3.8}$$

with

$$A = g^2 \frac{\rho_{\rm DM}}{x^2_{\rm t.o} m^2_{\rm n}}. \tag{3.9}$$

Setting the number of data points collected for a frequency f in an experiment to N, over a time period of T for the frequency bin, the time between data points is $\Delta t \left(= \frac{1}{f}\right)$. Since an experiment samples data points in a discrete manner one can rewrite the acceleration on the test object as time-series data. The acceleration for a data point, n, is then

$$a_n = \sqrt{A}\sum_j \alpha_j \sqrt{f_{\rm SHM}(v_j)\Delta v}\cdot \sin\left(m_{\rm DM}\left[1+\frac{v_j^2}{2}\right]n\Delta t+\phi_j\right), \tag{3.10}$$

with $n\Delta t = T$.

Taking the discrete Fourier transform of this:

$$a_k = \sum_{n=0}^{N-1} a_n e^{-2\pi i k n/N}, \tag{3.11}$$

one can find the PSD for the acceleration [6]:

$$S^k_{aa} = \frac{(\Delta t)^2}{T}\left|\sum_{n=0}^{N-1} a_n e^{-2\pi i k n/N}\right|^2, \tag{3.12}$$

with $k = 0$, ..., $N-1$ and $\omega = \frac{k2\pi}{T}$. Now setting

$$m_{\rm DM}\left(1+\frac{v_j^2}{2}\right) = \omega_j \tag{3.13}$$

the PSD in terms of ω_j and k becomes:

$$S^k_{aa} = A\frac{(\Delta t)^2}{T}\left|\sum_j \alpha_j \sqrt{f_{\rm SHM}(v_j)\Delta v}\sum_{n=0}^{N-1}\sin\left(\omega_j n\Delta t+\phi_j\right)e^{-2\pi i k n/N}\right|^2. \tag{3.14}$$

The PSD can be rewritten in terms of the experiment's angular frequency:

$$\omega = \frac{2\pi k}{\Delta t N} = \frac{2\pi k}{T}, \tag{3.15}$$

so that

$$S_{aa}(\omega) = A\frac{(\Delta t)^2}{T}\left|\sum_j \alpha_j\sqrt{f_{\mathrm{SHM}}(v_j)\Delta v}\sum_{n=0}^{N-1}\sin\left(\omega_j n\Delta t+\phi_j\right)e^{-i\omega n\Delta t}\right|^2. \tag{3.16}$$

Using that, for large T,

$$\begin{aligned}\frac{1}{T} = \Delta f &= \frac{1}{2\pi}\Delta\omega_j = \frac{1}{2\pi}\frac{m_{\mathrm{DM}}}{2}\Delta(v_j^2) \\ &= \frac{1}{2\pi}\frac{m_{\mathrm{DM}}}{2}\left((v_j+\Delta v)^2 - v_j^2\right) \approx \frac{1}{2\pi}m_{\mathrm{DM}}v_j\Delta v,\end{aligned} \tag{3.17}$$

where in the last step the fact that Δv^2 is almost zero has been used, results in a PSD of the form:

$$S_{aa}(\omega) = A\frac{m_{\mathrm{DM}}}{2\pi}\left|\sum_j \alpha_j\Delta v\sqrt{v_j f_{\mathrm{SHM}}(v_j)}\Delta t\sum_{n=0}^{N-1}\sin\left(\omega_j n\Delta t+\phi_j\right)e^{-i\omega n\Delta t}\right|^2. \tag{3.18}$$

Using this result and letting T approach infinity leads to the summation over j becoming an integral over v and Δt becoming an infinitesimal dt. This approximation is appropriate as a real experiment would run for a long enough time that the period would be huge in comparison to the time between data points. The PSD now only has one sum:

$$S_{aa}(\omega) = A\frac{m_{\mathrm{DM}}}{2\pi}\left|\int_0^\infty dv\alpha_v\sqrt{v f_{\mathrm{SHM}}(v)}dt\sum_{n=0}^{N-1}\sin\left(\omega_v ndt+\phi_v\right)e^{-i\omega ndt}\right|^2, \tag{3.19}$$

which can be calculated to:

$$\begin{aligned}&dt\sum_{n=0}^{N-1}\sin\left(\omega_v ndt+\phi_v\right)e^{-i\omega ndt} = \frac{dt}{2i}\sum_{n=0}^{N-1}\left\{e^{i(\omega_v-\omega)ndt}e^{i\phi_v} - e^{-i(\omega_v+\omega)ndt}e^{-i\phi_v}\right\} = \\ &= \frac{dt}{2i}\left\{e^{i\phi_v}\frac{1-e^{i(\omega_v-\omega)T}}{1-e^{i(\omega_v-\omega)dt}} - e^{-i\phi_v}\frac{1-e^{-i(\omega_v+\omega)T}}{1-e^{-i(\omega_v+\omega)dt}}\right\}.\end{aligned} \tag{3.20}$$

The exponential in the denominator can be Taylor expanded, since dt is so small that it can be reasonably assumed that

$$(\omega_v \pm \omega)dt << 1 \text{ and } (\omega_v \pm \omega)^2 dt^2 \approx 0, \tag{3.21}$$

yielding:

$$\begin{aligned}&dt\sum_{n=0}^{N-1}\sin\left(\omega_v ndt+\phi_v\right)e^{-i\omega ndt} \approx \frac{i}{2}\left\{e^{i\phi_v}\frac{1-e^{i(\omega_v-\omega)T}}{2i\cdot\frac{1}{2}(\omega_v-\omega)}+\right. \\ &\left.+\,e^{-i\phi_v}\frac{1-e^{-i(\omega_v+\omega)T}}{2i\cdot\frac{1}{2}(\omega_v+\omega)}\right\} = \frac{i}{2}\left\{-e^{i(\phi_v+(\omega_v-\omega)T/2)}\frac{e^{i(\omega_v-\omega)T/2}-e^{-i(\omega_v-\omega)T/2}}{2i\cdot\frac{1}{2}(\omega_v-\omega)}+\right. \\ &\left.+\,e^{-i(\phi_v+(\omega_v+\omega)T/2)}\frac{e^{i(\omega_v+\omega)T/2}-e^{-i(\omega_v+\omega)T/2}}{2i\cdot\frac{1}{2}(\omega_v+\omega)}\right\} \\ &= \frac{i}{2}e^{i(\phi_v+(\omega_v-\omega)T/2)}\left\{-\frac{\sin\left[\frac{1}{2}(\omega_v-\omega)T\right]}{\frac{1}{2}(\omega_v-\omega)} + e^{-i(2\phi_v+\omega_v T)}\cdot\frac{\sin\left[\frac{1}{2}(\omega_v+\omega)T\right]}{\frac{1}{2}(\omega_v-\omega)}\right\}.\end{aligned} \tag{3.22}$$

The final approximation for this sum requires using

$$(\omega_v \pm \omega)T \to \infty \tag{3.23}$$

with

$$\sin(x/\epsilon)/x \to \pi\delta(x) \text{ as } \epsilon \to 0, \tag{3.24}$$

yielding:

$$dt\sum_{n=0}^{N-1}\sin(\omega_v n dt + \phi_v)e^{-i\omega n dt} \approx \frac{i\pi}{2}e^{i[\phi_v+(\omega_v-\omega)T/2]}\left\{\delta\left(\frac{1}{2}(\omega_v-\omega)\right)+\right. \tag{3.25}$$
$$\left.+\, e^{-i[2\phi_v+\omega_v T]}\pi\delta\left(\frac{1}{2}(\omega_v+\omega)\right)\right\} = -i\pi e^{i[\phi_v+(\omega_v-\omega)T/2]}\delta(\omega_v-\omega).$$

In the last step, the second term with the Dirac delta function is discarded as the angular frequencies ω_v and ω have to be larger than zero.

The PSD then takes the final form:

$$S_{aa}(\omega) = A\frac{\pi}{2}\left| -i\int_0^\infty dv\alpha_v\sqrt{m_{\mathrm{DM}}vf_{\mathrm{SHM}}(v)}e^{i(\phi_v+(\omega_v-\omega)T/2)}\delta(\omega_v-\omega)\right|^2 = \tag{3.26}$$
$$= [d\omega = m_{\mathrm{DM}}vdv] = A\frac{\pi}{2}\left| -i\int_0^\infty d\omega\alpha_v\sqrt{\frac{f_{\mathrm{SHM}}(v)}{m_{\mathrm{DM}}v}}e^{i\phi_v}e^{\frac{i}{2}(\omega_v-\omega)T}\delta(\omega_v-\omega)\right|^2$$
$$= A\frac{\pi f_{\mathrm{SHM}}(v)}{2m_{\mathrm{DM}}v}\alpha^2\Big|_{v=\sqrt{2\omega/m_{\mathrm{DM}}-2}}.$$

Using that α is exponentially distributed, one can see that the PSD also follows this distribution, so that the distribution of the PSD is:

$$P[S_{aa}(\omega),\lambda(\omega)] = \frac{1}{\lambda(\omega)}e^{-S_{aa}(\omega)/\lambda(\omega)}, \tag{3.27}$$

with the mean $\lambda(\omega)$, and the mean of the total PSD,

$$\lambda_{\mathrm{tot}}(\omega) = \langle S_{aa}(\omega)\rangle + \lambda_{\mathrm{B}} = A\frac{\pi f(v)}{m_{\mathrm{DM}}v}\Big|_{v=\sqrt{2\omega/m_{\mathrm{DM}}-2}} + \lambda_{\mathrm{B}}, \tag{3.28}$$

where a background term λ_{B} has been taken into account, which has a Gaussian distribution.

The likelihood function for a data set d, given the model $\mathcal{M}$ (signal and background), and model parameters, θ, follow this same distribution as the PSD. For each data point, k, sampled at $\omega = \frac{2\pi k}{T}$ the wanted likelihood function then takes the form:

$$\mathcal{L}(d|\mathcal{M},\theta) = \prod_{k=1}^{N-1}\frac{1}{\lambda_{k,\mathrm{tot}}(\theta)}e^{-S_{aa}^{k,\mathrm{tot}}/\lambda_{k,\mathrm{tot}}(\theta)}. \tag{3.29}$$

Using this likelihood, it is possible to find the exclusion and discovery limits for the coupling constant determining the sensitivity of the experiment. Note that, like $x_{\mathrm{t.o}}$, the background is dependent on the experiment and can even be dependent on the frequency or the position of the test object depending on the experiment.

3.2 Exclusion and discovery limits

Finding exclusion and discovery limits for the coupling constant g can be done with the help of two test statistics, defined through the profile likelihood [6]. This function is two times the natural logarithm of the ratio between the likelihood for the signal plus background model $\mathcal{M}$ and the likelihood for a background only model $\mathcal{M}_{\mathrm{B}}$:

$$\Theta(m_{\mathrm{DM}}, A) = 2\{\ln[\mathcal{L}(d|\mathcal{M}, \{A, m_{\mathrm{DM}}, \hat{\theta}_{\mathrm{B}}\})] - \ln[\mathcal{L}(d|\mathcal{M}_{\mathrm{B}}, \hat{\theta}_{\mathrm{B}})]\}. \tag{3.30}$$

Note that the hat over the model parameters denotes that this background maximizes the background plus signal likelihood. The pair of test statistics used to find the exclusion and discovery limits are written as q_{exc} and q_{disc} respectively, and are calculated at 95% confidence interval and 5σ level, respectively. If $\hat{A}$ maximizes the profile likelihood, the test statistic for the exclusion limit is defined as:

$$q_{\mathrm{exc}}(m_{\mathrm{DM}}, A) = \begin{cases} \Theta(m_{\mathrm{DM}}, A) - \Theta(m_{\mathrm{DM}}, \hat{A}) & A \geq \hat{A}, \\ 0 & A < \hat{A}, \end{cases} \tag{3.31}$$

while the test statistic for the discovery limit is defined as:

$$q_{\mathrm{disc}}(m_{\mathrm{DM}}) = \Theta(m_{\mathrm{DM}}, \hat{A}). \tag{3.32}$$

The profile likelihood has the explicit form:

$$\Theta(m_{\mathrm{DM}}, A) = 2 \sum_{k=1}^{N-1} \left[S_{aa}^{k,\mathrm{tot}} \left(\frac{1}{\lambda_{\mathrm{B}}} - \frac{1}{\lambda_{k,\mathrm{tot}}} \right) - \log \frac{\lambda_{k,\mathrm{tot}}}{\lambda_{\mathrm{B}}} \right]. \tag{3.33}$$

By simulating data, $S_{aa}^{k,\mathrm{tot}}$, the test statistics and (by extension) the exclusion and discovery limits can be found. However, simulating with for example the Monte Carlo method is both time inefficient and computationally expensive [24]. The data can instead be asymptotically approximated with the so called Asimov data set.

3.2.1 The Asimov data set

The Asimov data set replaces the numerous simulated data sets with one "true" representation of the simulated data [24]. This means that the Asimov data set is the representation of the asymptotic data from the simulated data and can be used to derive expected experimental sensitivity analytically. Since the data set is the "true" data, there are no statistical fluctuations in the data set. When calculating the exclusion limit, a data set with no signal and only background should be viewed, meaning that A would be zero. When calculating the discovery limit though, the data set is still background only distributed, but with A instead maximizing the profile likelihood; the discovery limit needs to be exceeded for discovery since the background can *fake* a signal.

In order to write the test statistics with the Asimov data set, first the data set itself, $S_{aa}^{k,\mathrm{Asimov}}$, needs to be written. The true value of A is denoted as A_{t} and the true

value of the mean of the distribution is written in the same way. With this, the Asimov data of the acceleration is

$$S_{aa}^{k,\mathrm{Asimov}} \equiv \lambda_{k,\mathrm{t}} = A_{\mathrm{t}} \frac{\pi f(v) v}{m_{\mathrm{DM}}}\bigg|_{v=\sqrt{4\pi k/(m_{\mathrm{DM}}T)-2}} + \lambda_{\mathrm{B}}. \tag{3.34}$$

The reason that the Asimov PSD is equal to its mean is that the mean of the true data is itself, since there are no statistical fluctuations.

3.2.2 Deriving the exclusion and discovery limits

Using the Asimov data set, $\lambda_{k,\mathrm{t}}$, the asymptotic form of the profile likelihood can be found [6]:

$$\tilde{\Theta}(m_{\mathrm{DM}}, A) = 2 \sum_{k=1}^{N-1} \left[\lambda_{k,\mathrm{t}} \left(\frac{1}{\lambda_{\mathrm{B}}} - \frac{1}{\lambda_{k,\mathrm{tot}}} \right) - \ln \frac{\lambda_{k,\mathrm{tot}}}{\lambda_{\mathrm{B}}} \right]. \tag{3.35}$$

Here A_{t} maximizes the asymptotic form of the profile likelihood. Since a realistic experiment would have been run long enough that the width of the frequency bins would be much smaller than the range that λ_k and λ_{B} varies over, one can rewrite the sum to an integral using

$$2vdv = d(v^2) = \frac{4\pi}{m_{\mathrm{DM}}T} dk. \tag{3.36}$$

With eqs. (3.28) and (3.34) the asymptotic profile likelihood then looks like

$$\begin{aligned} \tilde{\Theta}(m_{\mathrm{DM}}, A) = \frac{T m_{\mathrm{DM}}}{\pi} \int_0^\infty dv v \Bigg\{ \left[A_{\mathrm{t}} \frac{\pi f_{\mathrm{SHM}}(v)}{m_{\mathrm{DM}} v \lambda_{\mathrm{B}}} + 1 \right] \cdot \left[1 - \frac{1}{1 + A \frac{\pi f_{\mathrm{SHM}}(v)}{m_{\mathrm{DM}} v \lambda_{\mathrm{B}}}} \right] + \\ - \ln \left[1 + A \frac{\pi f_{\mathrm{SHM}}(v)}{m_{\mathrm{DM}} v \lambda_{\mathrm{B}}} \right] \Bigg\}. \end{aligned} \tag{3.37}$$

With Taylor expansion to the second order, using

$$A \cdot \frac{\pi f_{\mathrm{SHM}}}{m_{\mathrm{DM}} v \lambda_{\mathrm{B}}} << 1, \text{ and} \tag{3.38}$$

$$A_{\mathrm{t}} \cdot \frac{\pi f_{\mathrm{SHM}}}{m_{\mathrm{DM}} v \lambda_{\mathrm{B}}} << 1, \tag{3.39}$$

with

$$A^3 \frac{\pi f_{\mathrm{SHM}}(v)}{m_{\mathrm{DM}} v \lambda_{\mathrm{B}}}^3 \to 0, \text{ and} \tag{3.40}$$

$$A_{\mathrm{t}} A^2 \frac{\pi f_{\mathrm{SHM}}(v)}{m_{\mathrm{DM}} v \lambda_{\mathrm{B}}}^3 \to 0, \tag{3.41}$$

the asymptotic profile likelihood simplifies to:

$$\begin{aligned}\tilde{\Theta}(m_{\mathrm{DM}}, A) \approx \frac{T m_{\mathrm{DM}}}{\pi} \int_0^\infty dv v \Bigg\{ \left[A_{\mathrm{t}} \frac{\pi f_{\mathrm{SHM}}(v)}{m_{\mathrm{DM}} v \lambda_{\mathrm{B}}} + 1 \right] \cdot \left[1 - 1 + A \frac{\pi f_{\mathrm{SHM}}(v)}{m_{\mathrm{DM}} v \lambda_{\mathrm{B}}} + \right. \\ \left. + A^2 \frac{\pi^2 f_{\mathrm{SHM}}(v)^2}{m_{\mathrm{DM}}^2 v^2 \lambda_{\mathrm{B}}^2} \right] - A \frac{\pi f_{\mathrm{SHM}}(v)}{m_{\mathrm{DM}} v \lambda_{\mathrm{B}}} + A^2 \frac{\pi^2 f_{\mathrm{SHM}}(v)^2}{2 m_{\mathrm{DM}}^2 v^2 \lambda_{\mathrm{B}}^2} \Bigg\} \approx \\ \approx \frac{\pi T}{m_{\mathrm{DM}}} A \left[A_{\mathrm{t}} - \frac{A}{2} \right] \int_0^\infty \frac{dv}{v} \frac{f_{\mathrm{SHM}}(v)^2}{\lambda_{\mathrm{B}}^2}.\end{aligned} \tag{3.42}$$

With this form of the profile likelihood and the definition of the exclusion limit test statistic in eq. (3.31), an expression for the test statistic can be found, with true value of the signal $A_{\mathrm{t}} = 0$ for background only:

$$q_{\mathrm{exc}} = -\frac{\pi T}{2 m_{\mathrm{DM}}} A^2 \int_0^\infty \frac{dv}{v} \frac{f_{\mathrm{SHM}}(v)^2}{\lambda_{\mathrm{B}}^2}. \tag{3.43}$$

Solving for the coupling constant, the exclusion limit g_{exc} can be found to be:

$$g_{\mathrm{exc}} = \frac{x_{\mathrm{t.o}} m_{\mathrm{n}}}{\sqrt{\rho_{\mathrm{DM}}}} \left[-q_{\mathrm{exc}} \frac{2 m_{\mathrm{DM}}}{\pi T} \left(\int_0^\infty \frac{dv}{v} \frac{f_{\mathrm{SHM}}(v)^2}{\lambda_{\mathrm{B}}^2} \right)^{-1} \right]^{\frac{1}{4}}. \tag{3.44}$$

In the same way, but with $A = A_{\mathrm{t}}$, the discovery limit test static as defined in eq. (3.32) can be found:

$$q_{\mathrm{disc}} = \frac{\pi T}{2 m_{\mathrm{DM}}} A_{\mathrm{t}}^2 \int_0^\infty \frac{dv}{v} \frac{f_{\mathrm{SHM}}(v)^2}{\lambda_{\mathrm{B}}^2}, \tag{3.45}$$

resulting in the discovery limit

$$g_{\mathrm{disc}} = \frac{x_{\mathrm{t.o}} m_{\mathrm{n}}}{\sqrt{\rho_{\mathrm{DM}}}} \left[q_{\mathrm{disc}} \frac{2 m_{\mathrm{DM}}}{\pi T} \left(\int_0^\infty \frac{dv}{v} \frac{f_{\mathrm{SHM}}(v)^2}{\lambda_{\mathrm{B}}^2} \right)^{-1} \right]^{\frac{1}{4}}. \tag{3.46}$$

3.2.3 Values of the exclusion and discovery limits

To confidently exclude a signal, one should do so at a confidence interval of 95% which corresponds to a p-value of $p = 0.05$ [25]. But to discover a signal one needs to take into account the look elsewhere effect (described in Section 3.2.3.2) and a confidence level of 5σ should be used as well. The p-value is then for the discovery limit $2.87 \cdot 10^{-7}$. In Section 3.2.3.1 the exclusion limit is found for the p-value of 0.05 and in Section 3.2.3.2 the discovery limit for a p-value of $2.87 \cdot 10^{-7}$ is found.

3.2.3.1 Exclusion limit at 95% confidence interval

When setting an exclusion limit, the p-value is one-sided since downward fluctuations in the measured acceleration would not be evidence against the background only hypothesis [25]. To find the numerical value for the test statistic $q_{\mathrm{exc}}^{95\%}$ corresponding

to this p-value, however, the cumulative distribution function (CDF), $F(q_{\text{exc}})$, of the test static, q_{exc}, needs to be found, since

$$p = 1 - F\left(q_{\text{exc}}\right). \tag{3.47}$$

To find the CDF the probability density function (PDF) must be integrated. The PDF for the test static is according to Wilks' theorem a half-chi squared distribution with one degree of freedom [6, 24]:

$$f\left(q_{\text{exc}}\right) = \frac{1}{2}\delta\left(-q_{\text{exc}}\right) + \frac{1}{2}\frac{1}{\sqrt{2\pi}}\frac{1}{\sqrt{-q_{\text{exc}}}}e^{q_{\text{exc}}/2}. \tag{3.48}$$

Note here that in the equation the negative value of the test static is taken and not the positive. This is because q_{exc} is at most zero and otherwise can only be negative from the definition in eq. (3.31), and can also be seen in eq. (3.43). With this expression, one can integrate to find that the CDF is

$$F\left(q_{\text{exc}}\right) = \Phi\left(\sqrt{-q_{\text{exc}}}\right), \tag{3.49}$$

where Φ is the standard normal distribution's CDF.

Finding the value of the test static at 95% confidence level now only takes setting the p-value to 0.05:

$$p = 0.05 = 1 - \Phi\left(\sqrt{-q_{\text{exc}}^{95\%}}\right) \implies \tag{3.50}$$

$$\implies q_{\text{exc}}^{95\%} = -(\Phi^{-1}(0.95))^2, \tag{3.51}$$

which can be found to be about -2.71. The exclusion limit at 95% confidence level is then:

$$g_{\text{exc}}^{95\%} = \frac{x_{\text{t.o}} m_{\text{n}}}{\sqrt{\rho_{\text{DM}}}}\left[2.71\frac{2m_{\text{DM}}}{\pi T}\left(\int_0^\infty \frac{dv}{v}\frac{f_{\text{SHM}}(v)^2}{\lambda_{\text{B}}^2}\right)^{-1}\right]^{\frac{1}{4}}. \tag{3.52}$$

In this thesis, the background is assumed to be constant in the potential experiment, leading to:

$$g_{\text{exc}}^{95\%} = \frac{x_{\text{t.o}} m_{\text{n}}\sqrt{\lambda_{\text{B}}}}{\sqrt{\rho_{\text{DM}}}}\left[2.71\frac{2m_{\text{DM}}}{\pi T}\left(\int_0^\infty \frac{dv}{v} f_{\text{SHM}}(v)^2\right)^{-1}\right]^{\frac{1}{4}} = \tag{3.53}$$

$$= \frac{x_{\text{t.o}} m_{\text{n}}\sqrt{\lambda_{\text{B}}}}{\sqrt{\rho_{\text{DM}}}}\left[2.71\frac{2m_{\text{DM}}}{\pi T}\frac{\sqrt{2\pi}v_0 v_{\text{obs}}}{\text{erf}(\sqrt{2}v_{\text{obs}}/v_0)}\right]^{\frac{1}{4}}.$$

where the integral evaluates to

$$\int_0^\infty \frac{dv}{v} f_{\text{SHM}}(v)^2 = \frac{\text{erf}(\sqrt{2}v_{\text{obs}}/v_0)}{\sqrt{2\pi}v_0 v_{\text{obs}}}. \tag{3.54}$$

The value of $x_{\text{t.o}}$ for the proposed experiment at CTH can be fixed using that the lead superconductive test object has an atomic mass of about 207.2 u. The constant

then has the value of 1.654952077. The values of the four backgrounds to be tested are $7 \cdot 10^{-16}$ m^3 s^{-4} Hz^{-1} $= 8.2 \cdot 10^{-49}$ eV, $8.2 \cdot 10^{-53}$ eV, $8.2 \cdot 10^{-55}$ eV, and $8.2 \cdot 10^{-59}$ eV. With the known values of the neutron mass and the local dark matter density, this leads to:

$$g_{\text{exc}}^{95\%} \approx 3.56 \cdot 10^{10} \text{ eV}^{-1} \cdot \sqrt{\lambda_{\text{B}}} \cdot \left[\frac{m_{\text{DM}}}{T}\right]^{1/4}. \tag{3.55}$$

Note that T is dependent on which independent mass frequency that is regarded, and on the experiment.

3.2.3.2 Discovery limit at the 5σ level

The p-value is also one sided in the case of the discovery limit, since upwards fluctuations in the measured acceleration would not be evidence against the background plus signal hypothesis [25]. Here, though, Wilks' theorem cannot be used directly to find the PDF as the discovery limit's associated test static has no degrees of freedom. But it is possible to show that this is also a half chi squared distribution, with the CDF $F\left(q_{\text{disc}}\right) = \Phi\left(\sqrt{q_{\text{disc}}}\right)$ [6]. The survival function can then be expressed as

$$S\left[q_{\text{disc}}^{5\sigma}\right] = 1 - \Phi\left(\sqrt{q_{\text{disc}}^{5\sigma}}\right), \tag{3.56}$$

which is the probability of finding a value higher than $q_{\text{disc}}^{5\sigma}$ given only background, i.e the probability of the background faking a signal. Getting a p-value from this, however, needs taking into account the look elsewhere effect.

The look elsewhere effect is an effect that occurs when much data is searched, which can cause a false conclusion of a signal since the number of searches in and of themselves may lead to an accidental fluctuation [6]. In this thesis, the signal is scanned for over several masses (frequencies) and the number of frequency bins would in a realistic experiment be big enough so that the look elsewhere effect would have an effect on the measured data.

The effect can be accounted for by using the relation between the survival function, the p-value and the number of independent mass points, $N_{m_{\text{DM}}}$. The number of independent mass points can be assumed to be huge. For one independent mass point the bandwidth is thought to be related to its escape velocity, $v_{\text{esc}} \approx v_0$, so that the difference between two subsequent mass points, m_{DM}^1 and m_{DM}^2 is $m_{\text{DM}}\alpha v_0^2$, with $\alpha \approx 3/4 \cdot v_{\text{obs}}/v_0 \approx 0.791$ being a number of order unity that is to be tuned to Monte Carlo simulations (not to be confused with the Rayleigh distributed random variable) [6]. The mass points can then be parameterised as:

$$m_{\text{DM}}^{(i)} = m_{\text{DM}}^{(0)} \cdot (1 + \alpha v_0^2)^i. \tag{3.57}$$

Using this, one can derive the approximate value of $N_{m_{\text{DM}}}$ by using the maximum

($f_{\max}$) and minimum ($f_{\min}$) frequencies scanned over:

$$\begin{aligned}\ln\left[\frac{f_{\max}}{f_{\min}}\right] = \ln\left[\frac{\omega_{\max}}{\omega_{\min}}\right] \approx \ln\left[(1+\alpha v_0^2)^{N_{m_{\mathrm{DM}}}-1}\right] = \\ = (N_{m_{\mathrm{DM}}}-1)\ln\left[1+\alpha v_0^2\right] \approx [N_{m_{\mathrm{DM}}} >> 1] \approx \\ \approx N_{m_{\mathrm{DM}}}\ln\left[1+\alpha v_0^2\right].\end{aligned} \tag{3.58}$$

With a Taylor expansion around $\alpha v_0^2 (<< 1)$ this becomes:

$$\ln\left[\frac{f_{\max}}{f_{\min}}\right] \approx N_{m_{\mathrm{DM}}}\alpha v_0^2 \implies N_{m_{\mathrm{DM}}} \approx \frac{1}{\alpha v_0^2}\ln\left[\frac{f_{\max}}{f_{\min}}\right]. \tag{3.59}$$

The relation between the p-value and $S\left[q_{\mathrm{disc}}^{5\sigma}\right]$ is

$$p = 1 - \left(1 - S\left[q_{\mathrm{disc}}^{5\sigma}\right]\right)^{N_{m_{\mathrm{DM}}}}. \tag{3.60}$$

Since p for a 5σ level is small (and by extension $S\left[q_{\mathrm{disc}}^{5\sigma}\right]$ as well), one can use a Taylor approximation of the first order to find:

$$p \approx N_{m_{\mathrm{DM}}} S\left[q_{\mathrm{disc}}^{5\sigma}\right]. \tag{3.61}$$

The value for the test statistic can then be found to be:

$$q_{\mathrm{disc}}^{5\sigma} = \left[\Phi^{-1}\left(1 - \frac{p}{N_{m_{\mathrm{DM}}}}\right)\right]^2 = \left[\Phi^{-1}\left(1 - \frac{2.87\cdot 10^{-7}}{\frac{1}{\alpha v_0^2}\ln[f_{\max}/f_{\min}]}\right)\right]^2. \tag{3.62}$$

Since this number, $N_{m_{\mathrm{DM}}}$, is experiment dependent, the discovery limit $g_{\mathrm{disc}}^{5\sigma}$ can only be expressed as:

$$g_{\mathrm{disc}}^{5\sigma} \approx 2.77\cdot 10^{10}\ \mathrm{eV}^{-1}\cdot\sqrt{\lambda_{\mathrm{B}}}\cdot\left[q_{\mathrm{disc}}^{5\sigma}\right]^{1/4}\cdot\left[\frac{m_{\mathrm{DM}}}{T}\right]^{1/4}, \tag{3.63}$$

with $q_{\mathrm{disc}}^{5\sigma}$ evaluated for the maximum and minimum frequency set by the experiment.

4

Results

In this chapter, the exclusion limit and the discovery limit are plotted against the mass for different backgrounds. Additionally, these plots are produced for two expressions for the time period in order to showcase the sensitivity dependence on the time period. This is done in Section 4.1. This is followed by a section on a comparison with the detection limit for the vector boson for an experiment with optomechanical sensors from Figure 4 in [5]. The comparison is done for the two most optimistic backgrounds and for both types of expression for the time period. This is done in Section 4.2. The chapter is concluded with Section 4.3, which discusses the results and offers a conclusion.

4.1 Plots of the exclusion and discovery limits

The 5σ discovery limit and the 95% exclusion limit were plotted against the mass for masses realistic for the experiment. The mass range plotted over was dependent on the frequency range the experiment is likely to be able to probe, i.e. from 30 Hz to an optimistic 1 kHz (a more pessimistic highest frequency would be 200 Hz). This corresponds to a mass range between $1.24 \cdot 10^{-13}$ eV and $4.14 \cdot 10^{-12}$ eV, but with a more pessimistic upper limit of $8.27 \cdot 10^{-13}$ eV. The period for each frequency bin was set based on the mass related to that frequency bin. Two ways of formulating this relations were probed; one where the time period was proportional to the m_{DM}^{-1} and one where the period was proportional to m_{DM}^{-5}, both with the maximum time period of 1000 s for the smallest mass. As such, the time periods T_{-1} and T_{-5} can be written as the following functions, with $m_{\mathrm{DM},i}$ being the initial mass,

$$T_{-1} = 1000 \text{ s} \cdot m_{\mathrm{DM},i} \cdot m_{\mathrm{DM}}^{-1} \tag{4.1}$$

and

$$T_{-5} = 1000 \text{ s} \cdot m_{\mathrm{DM},i}^{5} \cdot m_{\mathrm{DM}}^{-5} \tag{4.2}$$

This was plotted for all four proposed background terms. Note that the plotted exclusion limits are dashed lines while the plots of the discovery limits are solid, and that the plots of the limits are red for the experiments where the test object has a radius of 1 µm and blue for the test object with a radius of 100 µm. The lines are also slightly transparent for the optimistic value of the quality factor. The highest mass which can be said to be realistic to probe is marked with a grey dashed line.

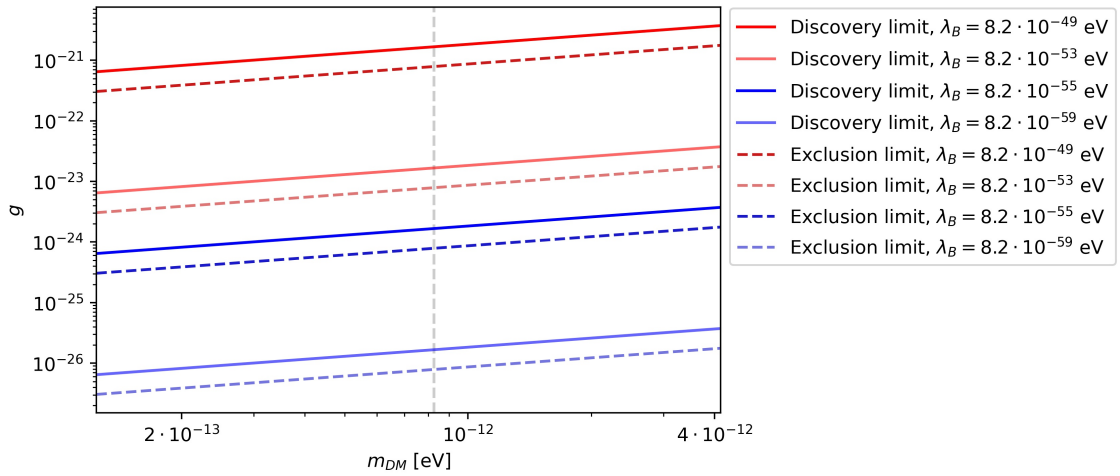

Figure 4.1: The exclusion limit of the coupling constant at 95% confidence level and the discovery limit at the 5σ level plotted against m_{DM} for four backgrounds, marked with dashed lines and solid lines respectively. The time period used for each frequency bin follows eq. (4.1), with an initial mass of $1.24 \cdot 10^{-13}$ eV. The period of the highest probed frequency bin was about 29.95 s. The plotted lines are red and blue depending on whether the background term is for a test object with the radius of 1 µm or 100 µm respectively. The lines are slightly transparent for the optimistic value of the quality factor. The vertical line shows the lowest mass that is in the optimistic part of the mass range.

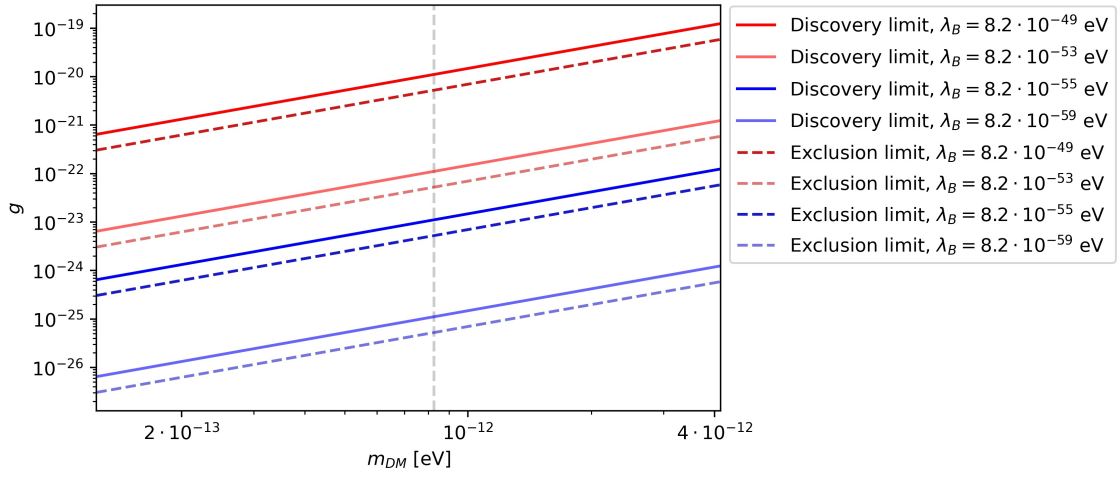

Figure 4.2: The exclusion limit of the coupling constant at 95% confidence level and the discovery limit at the 5σ level plotted against m_{DM} for four backgrounds, marked with dashed lines and solid lines respectively. The time period used for each frequency bin follows eq. (4.2), with an initial mass of $1.24 \cdot 10^{-13}$ eV. The period of the highest probed frequency bin was about 24.1 µs. The plotted lines are red and blue depending on whether the background term is for a test object with the radius of 1 µm or 100 µm respectively. The lines are slightly transparent for the optimistic value of the quality factor. The vertical line shows the lowest mass that is in the optimistic part of the mass range.

Additionally, all the plots are logarithmized. Figure 4.1 shows the plots together for the time period proportional to one over the dark matter mass. The discovery and the exclusion limits are proportional to the square root of the mass to the square root of the background. Figure 4.2 shows the plots together for the time period proportional to one over the dark matter mass to the power of five. The discovery and the exclusion limits are proportional to the square root of the mass to the power three, and also to the square root of the background.

As in Chapter 2 and 3, the dark matter density has been set to 0.4 GeV/cm^3, $x_{\text{t.o}}$ has been set to 1.65, while α has been set to 0.791, and the velocity distribution from the standard halo model has been used. The values of v_0 and v_{obs} where $7.338 \cdot 10^{-4}$, which is approximately 220 km/s, and $7.738 \cdot 10^{-4}$, which is approximately 232 km/s respectively.

4.2 Comparison with an experiment that makes use of mechanical quantum sensors

To get an understanding of the sensitivity of this potential experiment it needs to be compared to other experiments. A comparison here could showcase what parameters are most important to perfect in order to get the best sensitivity for finding the vector bosonic dark matter candidate of focus in this thesis. Such an experiment using optomechanical sensors is discussed for the same dark matter candidate in the article [5]. In Figure 4 in that article, a discovery limit of the resonant scan at the standard quantum limit is shown, which can be compared to the limits from this thesis. The discovery limit for this optomechanical experiment had a background depending on both thermal effects and effects from the standard quantum limit at resonance.

The plots of the discovery and exclusion limits for the potential experiment using levitated bodies were made in the same way as in Section 4.1. The same values and the same functions of the time periods were used, and the same mass range. Only the exclusion and discovery limits for the background based on the test object with a radius of 100 µm were used, though, to ease comparison with the resonant standard quantum limit scan in Figure 4 in [5].

The data from the plot in Figure 4 in [5] was extracted using a plot digitizer from `https://apps.automeris.io/wpd/`. Then this data is plotted inside of the relevant mass range with the calculated discovery and exclusion limits for the hypothetical experiment using magnetomechanics. The discovery limit from the optomechanical experiment is plotted with a solid green line and the discovery limit and the exclusion limit for the magnetomechanical experiment are plotted with solid blue lines and dashed blue line respectively, with the lines that are slightly transparent being for the background with the more optemistic quality factor. Figure 4.3 show this for the case where the time period follows eq. (4.1) and Figure 4.4 show this for the case where the time period follows eq. (4.2).

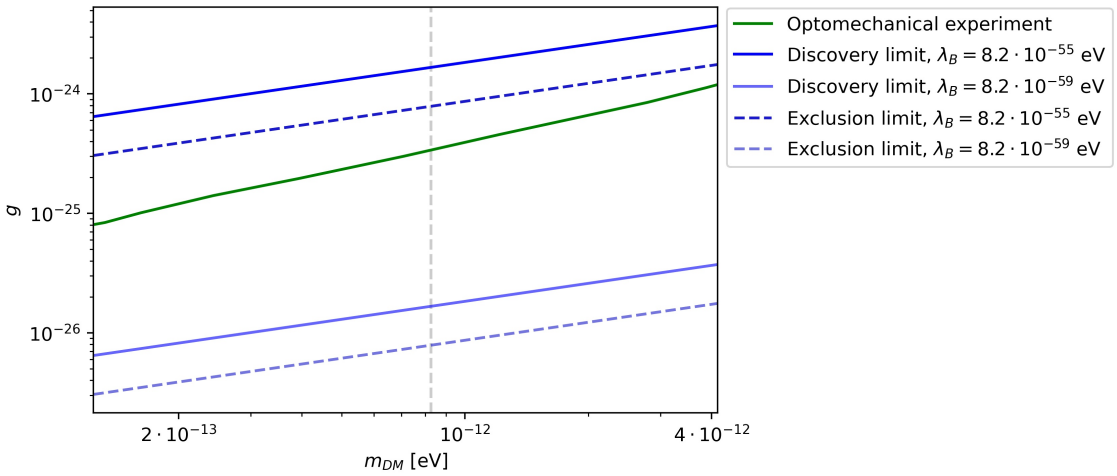

Figure 4.3: The exclusion limit of the coupling constant at 95% confidence level and discovery limit at the 5σ level plotted against m_{DM} for four backgrounds, marked with dashed lines and solid lines respectively. The time period used for each frequency bin follows eq. (4.1), with an initial mass of $1.24 \cdot 10^{-13}$ eV. The period of the highest probed frequency bin was about 29.95 s. The test object had a radius of 100 µm. The blue lines shows the exclusion and discovery limits for the magnetomechanical experiment and the green line show the discovery limit for the optomechanical experiment. The lines are slightly transparent for the optimistic value of the quality factor. The vertical line shows the highest non-optimistic mass.

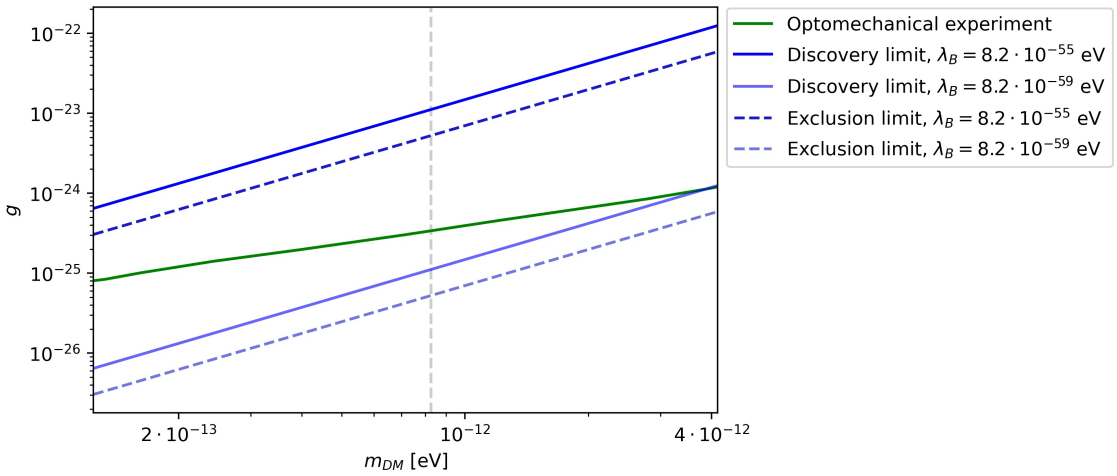

Figure 4.4: The exclusion limit of the coupling constant at 95% confidence level and discovery limit at the 5σ level plotted against m_{DM} for four backgrounds, marked with dashed lines and solid lines respectively. The time period used for each frequency bin follows eq. (4.2), with an initial mass of $1.24 \cdot 10^{-13}$ eV. The period of the highest probed frequency bin was about 24.1 µs. The test object had a radius of 100 µm. The blue lines shows the exclusion and discovery limits for the magnetomechanical experiment and the green line show the discovery limit for the optomechanical experiment. The lines are slightly transparent for the optimistic value of the quality factor. The vertical line shows the highest non-optimistic mass.

4.3 Discussion

In this section the results presented in the two previous sections are discussed and lastly a conclusion for the thesis is presented. The first section discusses the assumptions made in this thesis and how they have affected the results.

4.3.1 Framework for the experiment

Some relevant assumptions made in this thesis is of course the values of constants that have been used, such as ρ_{DM} and the α based on from Monte Carlo simulations done in [6]. However most of these can be easily modified if a more accurate estimation of the value was to be found, and the overall form of the plots would not differ from this.

Also the models used have had a great effect on the results, as the difference from the different background terms can attest to. If there are bigger contributions to the background then the ones assumed it could change the plots drastically, especially if the background has a dependence on the frequency of the dark matter wave. Though with this experiment being hypothetical this is an acceptable approximation since the goal of this thesis is to test the possible sensitivity and the difference of the effect from the most conservative and the most optimistic backgrounds are of five orders of magnitude.

The dependence of the time period on the mass scanned over is clearly relevant as the inclination of the plots is changed quite noticeably. The two models tested for this also have greatly different effects on the lowest time scanned over. This is notable since an assumption made in Chapter 3 is that $T \to \infty$ for each mass bin, and for a strong enough dependence on the mass and a big enough mass range to scan over, this assumption is incorrect.

The assumption that the dark matter velocity adheres to the standard halo model is also made, and thus some changes would have to be done (specifically in eq. (3.54)) in case a significantly different model was to be proposed.

In the end a change in the background term has a fairly small effect on the overall sensitivity of the experiment since the square root of the background term is used. It should be noted that the change between optimistic quality factor and the mass (size) change of the test object is greatly favourable to a background with a bigger test object.

4.3.2 Comparison with the optomechanical experiment

From the comparison it is clear that only the two most optimistic estimates on the sensitivity is near the sensitivity of the optomechanical experiment. The estimations of the sensitivity that are close to the discovery limit estimation from [5] are the ones that have the background being based on the test object having a radius of 100 µm.

As can be seen in the figures (4.3 and 4.4) the inclinations of the plotted limits are quite relevant as a stronger mass dependence for the time period could mean that the most optimistic estimate goes from having a higher sensitivity then the estimated discovery limit from [5]for lower frequencies, to intersect the limit and then having a lower sensitivity than limit at higher frequencies. The higher frequencies can as such be less relevant than the lower frequencies depending on how the time period is related to the scanned frequency. It should also be noted that experimentation on the higher frequency is optimistic.

4.3.3 Conclusion

The estimated sensitivity from this thesis does show that discovery in this mainly unexplored realm of dark matter can be possible for a coupling constant with a order of magnitude as low as -26 to -22. Even though only the most optimistic estimates on the sensitivity came close to the discovery limit estimated in [5], the comparison does show that it is possible to get a better sensitivity with this style of experiment as long as the experiment is tuned to do this, with a greater focus on getting more massive test objects and some focus on getting a higher value for the quality factor. Though depending on how the time period is related to the frequency bin focusing on reaching higher masses with this experiment can yield limited gains. Still this thesis motivates testing and improving the experiment with levitated magnetomechanics.

Bibliography

[1] G. Bertone and D. Hooper, "History of dark matter," *Rev. Mod. Phys.*, vol. 90, 2018. [Online]. Available: https://doi.org/10.1103%2Frevmodphys.90.045002

[2] G. Bertone, "The moment of truth for WIMP dark matter," *Nature*, vol. 468, 2010. [Online]. Available: https://doi.org/10.1038%2Fnature09509

[3] T. M. Undagoitia and L. Rauch, "Dark matter direct-detection experiments," *J. Phys. G*, vol. 43, 2015. [Online]. Available: https://doi.org/10.1088%2F0954-3899%2F43%2F1%2F013001

[4] P. W. Graham, D. E. Kaplan, J. Mardon, S. Rajendran, and W. A. Terrano, "Dark matter direct detection with accelerometers," *Phys. Rev. D*, vol. 93, 2016. [Online]. Available: https://doi.org/10.1103%2Fphysrevd.93.075029

[5] D. Carney, A. Hook, Z. Liu, J. M. Taylor, and Y. Zhao, "Ultralight Dark Matter Detection with Mechanical Quantum Sensors," *New J. Phys.*, vol. 23, 2021. [Online]. Available: https://doi.org/10.1088%2F1367-2630%2Fabd9e7

[6] J. W. Foster, N. L. Rodd, and B. R. Safdi, "Revealing the Dark Matter Halo with Axion Direct Detection," *Phys. Rev. D*, vol. 97, 2018. [Online]. Available: https://doi.org/10.1103%2Fphysrevd.97.123006

[7] L. Hui, "Wave Dark Matter," *Annu. Rev. Astron. Astrophys.*, vol. 59, 2021. [Online]. Available: https://doi.org/10.1146%2Fannurev-astro-120920-010024

[8] F. Zwicky, "The redshift of extragalactic nebulae," *Helv. Phys. Acta*, vol. 6, 1933, Translated by David Parker. [Online]. Available: http://spiff.rit.edu/classes/phys440/lectures/gal_clus/zwicky_1933_en.pdf

[9] A. Choudhuri, "Extragalactic astronomy," in *Astrophysics for Physicists*, Cambridge University Press, 2010, pp. 261–296.

[10] P. Tisserand et al. (EROS-2 coll.), "Limits on the Macho content of the Galactic Halo from the EROS-2 Survey of the Magellanic Clouds," *Astron. Astrophys.*, vol. 469, 2007. [Online]. Available: https://doi.org/10.1051%2F0004-6361%3A20066017

[11] P. A. R. Ade et al. (Planck coll.), "Planck 2015 results. XIII. Cosmological parameters," *Astron. Astrophys.*, vol. 594, 2016. [Online]. Available: https://doi.org/10.1051%2F0004-6361%2F201525830

[12] A. Choudhuri, "The thermal history of the Universe," in *Astrophysics for Physicists*, Cambridge University Press, 2010, pp. 325–355.

[13] A. Arbey and F. Mahmoudi, "Dark matter and the early Universe: A review," *Prog. Part. Nucl. Phys.*, vol. 119, 2021. [Online]. Available: https://doi.org/10.1016%2Fj.ppnp.2021.103865

[14] W. Wieczorek, "Wieczorek lab," [Online; accessed 6 November 2023]. Available: https://wieczorek-lab.com/.

[15] M. Gutierrez Latorre, G. Higgins, A. Paradkar, T. Bauch, and W. Wieczorek, "Superconducting Microsphere Magnetically Levitated in an Anharmonic Potential with Integrated Magnetic Readout," *Phys. Rev. Appl.*, vol. 19, 2023. [Online]. Available: https://link.aps.org/doi/10.1103/PhysRevApplied.19.054047

[16] P. de Salas, K. Malhan, K. Freese, K. Hattori, and M. Valluri, "On the estimation of the local dark matter density using the rotation curve of the Milky Way," *J. Cosmol. Astropart. Phys.*, vol. 2019, 2019. [Online]. Available: https://doi.org/10.1088%2F1475-7516%2F2019%2F10%2F037

[17] E. G. M. Ferreira, "Ultra-light dark matter," *Astron. Astrophys. Rev.*, vol. 29, 2021. [Online]. Available: https://doi.org/10.1007%2Fs00159-021-00135-6

[18] F. Mandl and G. Shaw, "QED Processes in Lowest Order," in *Quantum Field Theory*, 2nd ed. John Wiley & Sons, Ltd, 2010, pp. 127–158.

[19] M. Cirelli, E. D. Nobile, and P. Panci, "Tools for model-independent bounds in direct dark matter searches," *J. Cosmol. Astropart. Phys.*, vol. 2013, 2013. [Online]. Available: https://doi.org/10.1088%2F1475-7516%2F2013%2F10%2F019

[20] E. Merzbacher, "Time-Dependent Perturbation Theory," in *Quantum Mechanics*, 3rd ed. John Wiley & Sons, Inc, 1998, pp. 482–516.

[21] ——, "The Formal Theory of Scattering," in *Quantum Mechanics*, 3rd ed. John Wiley & Sons, Inc, 1998, pp. 517–534.

[22] J. Frerick, J. Jaeckel, F. Kahlhoefer, and K. Schmidt-Hoberg, "Riding the dark matter wave: Novel limits on general dark photons from LISA Pathfinder," 2024. [Online]. Available: http://dx.doi.org/10.1016/j.physletb.2023.138328

[23] P. Beckmann, "Rayleigh Distribution and Its Generalizations," *J. Res. Natl. Inst. Stand. Technol.*, vol. 68D, 1964. [Online]. Available: https://nvlpubs.nist.gov/nistpubs/jres/68D/jresv68Dn9p927_A1b.pdf

[24] G. Cowan, K. Cranmer, E. Gross, and O. Vitells, "Asymptotic formulae for likelihood-based tests of new physics," *Eur. Phys. J. C*, vol. 71, 2011. [Online]. Available: https://arxiv.org/abs/1007.1727

[25] E. Gross, "Practical Statistics for High Energy Physics," *CERN Yellow Rep.: Sch. Proc.*, vol. 3, 2018. [Online]. Available: https://e-publishing.cern.ch/index.php/CYRSP/article/view/1124

DEPARTMENT OF PHYSICS
CHALMERS UNIVERSITY OF TECHNOLOGY
Gothenburg, Sweden
www.chalmers.se

CHALMERS
UNIVERSITY OF TECHNOLOGY